

## The Pore-Lining Region of Shaker Voltage-Gated Potassium Channels: Comparison of $\beta$ -Barrel and $\alpha$ -Helix Bundle Models

Ian D. Kerr and Mark S. P. Sansom

Laboratory of Molecular Biophysics, The University of Oxford, Oxford OX1 3QU, England

**ABSTRACT** Although there is a large body of site-directed mutagenesis data that identify the pore-lining sequence of the voltage-gated potassium channel, the structure of this region remains unknown. We have interpreted the available biochemical data as a set of topological and orientational restraints and employed these restraints to produce molecular models of the potassium channel pore region, H5. The H5 sequence has been modeled either as a tetramer of membrane-spanning  $\beta$ -hairpins, thus producing an eight-stranded  $\beta$ -barrel, or as a tetramer of incompletely membrane-spanning  $\alpha$ -helical hairpins, thus producing an eight-staved  $\alpha$ -helix bundle. In total, restraints-directed modeling has produced 40 different configurations of the  $\beta$ -barrel model, each configuration comprising an ensemble of 20 structures, and 24 different configurations of the  $\alpha$ -helix bundle model, each comprising an ensemble of 24 structures. Thus, over 1300 model structures for H5 have been generated. Configurations have been ranked on the basis of their predicted pore properties and on the extent of their agreement with the biochemical data. This ranking is employed to identify particular configurations of H5 that may be explored further as models of the pore-lining region of the voltage-gated potassium channel pore.

### INTRODUCTION

Despite impressive advances in the determination of the structure of membrane proteins (e.g., Iwata et al., 1995; Tsukihara et al., 1996) the number of high-resolution structures remains small. However, for a growing number of membrane proteins, there is an accumulation of biochemical and site-directed mutagenesis data that may contain direct or indirect structural information. For example, site-directed mutagenesis (reviewed in Hucho et al., 1996) and electron microscopy (Unwin, 1993, 1995) of the nicotinic acetylcholine receptor have identified the pore-lining sequences and suggested their secondary structural conformation. Furthermore, mutagenesis combined with spin-labeling and fluorescence energy resonance data has suggested possible three-dimensional models for the transmembrane helices of *Escherichia coli* lac permease (Wu and Kaback, 1996). In this paper we attempt to integrate the results of site-directed mutagenesis data into molecular models of the pore of the voltage-gated potassium channel.

Potassium channels are responsible for the selective flux of potassium ions across the cell membrane of virtually all organisms (Hille, 1992). They are ubiquitous, being found in both excitable and nonexcitable cells, and are responsible for the maintenance of the resting membrane potential, as well as the hyperpolarization of membranes during action potentials. Sequences encoding potassium-selective channels have been cloned from mammals (Frech et al., 1989), insects (Tempel et al., 1987), plants (Schachtman et al.,

1992), and bacteria (Milkman, 1994). Potassium channels have recently been classified into two families on the basis of their proposed membrane topologies. The voltage-gated (Kv) family of potassium channels (Gutman and Chandy, 1993) is characterized by a proposed membrane topology of six transmembrane (TM)  $\alpha$ -helices (S1–S6), and a further transmembrane region H5 (sometimes called the P-region or SS1–SS2), which is located between S5 and S6. The S4 helix contains a positively charged residue at every third position and acts as the primary voltage-sensing element. The inward-rectifier family (Kir) of potassium channels (Doupnik et al., 1995) has a simpler proposed transmembrane topology, with two TM  $\alpha$ -helices (M1 and M2) on either side of a region homologous to H5 (Ho et al., 1993; Kubo et al., 1993). Thus the M1-H5-M2 region of Kir channels is believed to be analogous to the S5-H5-S6 region of Kv channels (Aldrich, 1993). Both Kv and Kir channels are believed to form tetramers (MacKinnon, 1991; Li et al., 1994; Yang et al., 1995). More recently, a number of potassium channels have been cloned with two M1-H5-M2 regions adjacent in their sequence (Ketchum et al., 1995; Lesage et al., 1996). These may define a further family of potassium channels.

Currently there are no three-dimensional structural data for Kv channels that may be used to explain their function. However, the expression of cloned Kv channels and the investigation of expressed channels by patch-clamp methods have made it possible to accumulate a large body of functional data (Pongs, 1992). Moreover, the expression and characterization of site-directed mutants, and more recently the application of the cysteine-scanning mutagenesis technique have produced a considerable body of data (Brown, 1993). Such data may contain indirect information on both the structure of the pore domain and the mechanisms underlying voltage gating.

Received for publication 26 February 1997 and in final form 13 May 1997.

Address reprint requests to Dr. M. S. P. Sansom, Laboratory of Molecular Biophysics, The University of Oxford, The Rex Richards Building, South Parks Road, Oxford OX1 3QU, England. Tel.: 44-1865-275371; Fax: 44-1865-275182; E-mail: mark@biop.ox.ac.uk.

© 1997 by the Biophysical Society

0006-3495/97/08/581/22 \$2.00

A substantial number of site-directed mutagenesis studies have focused on the H5 region situated between S5 and S6 in the Kv channel sequence. This 21-residue region is the most highly conserved sequence within the potassium channel superfamily. It has been successfully employed as a target search sequence in automated searches of amino acid and nucleotide sequence data bases in attempts to identify novel potassium channels (Ketchum et al., 1995; Lesage et al., 1996). Mutagenesis data have identified the H5 region as the primary determinant of ionic selectivity and of susceptibility to the channel blocker tetraethylammonium (TEA). H5 has been found to play a role in Kv channel block by scorpion protein toxins such as charybdotoxin (CTX) (MacKinnon and Miller, 1989; Hartmann et al., 1991; Kirsch et al., 1992; Tagliatalata et al., 1993). It has also been suggested that this 21-residue region spans the membrane twice, as residues at the start and end of the sequence lie at the extracellular mouth of the channel, and residues at the midpoint of H5 contribute to the intracellular mouth of the channel (Yellen et al., 1991; Yool and Schwarz, 1991). More recently, it has been demonstrated that residues in the S5 and S6 regions may also be exposed to the pore (Lopez et al., 1994; Shieh and Kirsch, 1994; Tagliatalata et al., 1994).

The key role of H5 in Kv channel function has inspired a number of molecular modeling studies based on different underlying structural motifs. Both long-pore (Bogusz et al., 1992; Jin and Weaver, 1993; Bradley and Richards, 1994; Lipkind et al., 1995) and short-pore (Durell and Guy, 1996) models for the H5 region have been proposed. The central H5 region of these has been modeled variously as an anti-parallel  $\beta$ -hairpin (Bogusz et al., 1992; Bradley and Richards, 1994), an  $\alpha$ -helix-turn-random coil conformation (Durell and Guy, 1996), and a  $\beta$ -strand-turn-random coil conformation (Lipkind et al., 1995). Although all of these models have their merits, it is evident that a somewhat more wide-ranging and systematic comparison of possible models is called for.

In this communication we present an alternative, more automated approach to modeling the Kv channel H5 region. We present an analysis of the current site-directed and cysteine-scanning mutagenesis, which is interpreted as a series of restraints that any valid Kv channel model should satisfy. Two structurally distinct families of Kv channel pore-region models are generated: 1) eight-stranded  $\beta$ -barrel models, in which each H5 unit adopts a membrane-spanning  $\beta$ -hairpin conformation; and 2) eight-staved  $\alpha$ -helix bundle models, in which each H5 region adopts a partially membrane-spanning  $\alpha$ -helical hairpin conformation. For each structural class of model ( $\alpha$ -helix bundle versus  $\beta$ -barrel), a number of different configurations can be defined. Analysis of the 42 possible  $\beta$ -barrel and 24 possible  $\alpha$ -helix bundle configurations identifies the most plausible models, which can be investigated further as candidate structures for the narrowest region of the Kv channel pore.

## METHODS

### Programs

Distance geometry, simulated annealing, and restrained molecular dynamics simulations were performed using Xplor version 3.1 (Brünger, 1992), running on a DEC Alphaserver 2100 4/275 or Silicon Graphics Indigo2 workstation. Distance geometry (DG) calculations were performed with an all-atom representation (PARALLHDG parameter set), and simulated annealing and molecular dynamics were performed with extended atoms for nonpolar hydrogens (PARAM19 parameter set; Brooks et al., 1983). This switch in parameter sets was justified, because the PARALLHDG set is parameterized for DG calculations, whereas PARAM19 is more suited to conventional MD. Manipulation and visualization of structures was performed with Quanta v4.0 (Molecular Simulations, Waltham, MA) and Rasmol v2.6 (Roger Sayle, Glaxo-Wellcome). Pore radius profiles were calculated with the program HOLE (Smart et al., 1993), and stereochemistry was analyzed with Procheck (Morris et al., 1992). Additional analysis was performed either with Xplor or with programs written in Fortran 77.

### Simulated annealing via molecular dynamics

Final models for both  $\beta$ -barrels and  $\alpha$ -helix bundles were generated from templates by simulated annealing via restrained molecular dynamics (SA/MD). The generation of templates for  $\beta$ -barrel models is described below, and the generation of templates for  $\alpha$ -helix bundle models is described in the Results. We have adopted the SA/MD procedure employed to model the leucine zipper of the GCN4 transcriptional activator (Nilges and Brünger, 1991), and have previously described in detail our implementation of SA/MD in molecular modeling studies of a number of ion channel systems (Kerr et al., 1994; Breed et al., 1995, 1997; Mitton and Sansom, 1996; Sankaramakrishnan et al., 1996). Briefly, structures were grown from fixed template atoms (excluding loop template atoms, which were unrestrained) by molecular dynamics at 1000 K. During this period, energy terms for bond lengths and bond angles were gradually introduced, followed by terms for dihedral and improper torsion angles. Once side-chain atoms had been generated, loop atoms were released from constraints, and a repulsive van der Waals potential was introduced as the structures were slowly cooled to 300 K at intervals of 25 K. No electrostatic terms were present during this stage. From each template,  $m$  structures were generated by repeat runs of simulated annealing.

Stage 2 of SA/MD consisted of a 4-ps molecular dynamics simulation during which the temperature was cooled from 500K to 300K, and template atoms were released from initial restraints. During this phase electrostatic terms were also introduced by the scaling of partial atomic charges on polar and charged side chains from 5% to 42% of their full values in the PARAM19 parameter set. After cooling to 300

K, 5 ps of unrestrained molecular dynamics was performed, followed by 2000 steps of conjugate gradient energy minimization. For each structure generated by simulated annealing,  $n$  structures were generated by independent MD runs, yielding a total of  $m \times n$  structures (Kerr et al., 1994).

During SA/MD, restraints were applied to models to retain the desired configuration. For  $\beta$ -barrel models, restraints were as described for distance geometry calculations (see below). For  $\alpha$ -helix bundles,  $\alpha$ -helicity was maintained by distance restraints between the O atom of residue  $i$  and the H atom of residue  $i + 4$ . Target distances for these restraints were  $2.06 \pm 0.32 \text{ \AA}$  (Baker and Hubbard, 1984). A single distance restraint with a target distance of  $10.5 \text{ \AA}$  acted between the geometric centers of neighboring  $\alpha$ -helices to retain overall bundle structure.

### Generation of $\beta$ -barrel model templates

Distance geometry and simulated annealing (DG/SA) were employed to generate  $\beta$ -barrel structural templates for further refinement by simulated annealing and molecular dynamics. Input restraints for DG/SA calculations consisted of a molecular structure file (which specifies the covalent structure), dihedral angle restraints, hydrogen bond distance restraints, and cross-pore distance restraints. In DG/SA, Ala<sup>21</sup> models were constructed (i.e., containing backbone and C $\beta$  atoms only) because the experimentally derived restraints provide no information on possible side-chain conformations. DG/SA consisted of two stages, an embedding stage and a simulated annealing regularization stage. In the embedding stage, the restraints (above) are used to produce a distance matrix for all atom pairs  $ij$  in the H5 tetramer. One hundred solutions to this matrix were determined by standard distance geometric methods (Kuntz et al., 1989) implemented in Xplor (Brünger, 1992). Of these, ~50% were discarded as having the wrong chirality (i.e., in the case of  $\beta$ -barrels, negative shear numbers; Murzin et al., 1994). The regularization stage consisted of a short burst of simulated annealing via molecular dynamics, cooling the structure from an initial temperature of 2000 K to a final temperature of 100 K, while increasing the weight applied to a repulsive van der Waals potential.

### Prediction of conductance

Conductances were predicted by treating pores as an irregular cylinder with radius  $r(z)$  (derived with HOLE; Smart et al., 1993), filled with an electrolyte of resistivity  $\rho$ . For a pore running from  $z = a$  to  $z = b$ , a reasonable approximation to the electrical resistance of the pore may be obtained by integrating  $\rho/(\pi r^2)$  along its length (Hille, 1992; Sansom and Kerr, 1995), and the pore conductance obtained by the reciprocal of this is

$$G_{\text{pore}} = \left[ \int_a^b \frac{\rho}{\pi r^2} dz \right]^{-1}$$

If the radii at the mouths of the pore are given by  $r(a)$  and  $r(b)$ , then an access resistance can be written as

$$G_{\text{access}} = \frac{\rho}{4r(a)} + \frac{\rho}{4r(b)}$$

The upper limit upon the pore conductance is thus obtained as  $G_{\text{upper}} = G_{\text{pore}} + G_{\text{access}}$ . The value for  $G_{\text{upper}}$  can be corrected by dividing by a scale factor  $s$ , where  $s$  is derived from analysis of ion channels with known structure and conductance (Smart et al., 1997). A value of  $s = 5$  was employed to produce values for predicted conductance, i.e.,  $G_{\text{pred}} = G_{\text{upper}}/5$ .

## RESULTS

Although mutagenesis has been performed on a variety of Kv channels from different species, we have assumed that data obtained on, for example, Kv2.1 are applicable to all Kv channels. The extremely high conservation of the H5 region across the Kv channel family supports the validity of this assumption. Thus the H5 sequence from *Shaker-A* (Tempel et al., 1987) was employed in all modeling studies:

1            5            10            15            21  
P-D-A-F-W-W-A-V-V-T-M-T-T-V-G-Y-G-D-M-T-P

Pro<sup>1</sup> and Pro<sup>21</sup> correspond to Pro<sup>430</sup> and Pro<sup>450</sup>, respectively, in the full-length protein. The sequence was blocked with an acetyl group at the N-terminus and an amide at the C-terminus to mimic the presence of peptide bonds at either end of H5 in the intact protein.

### Interpretation of site-directed and cysteine-scanning mutagenesis on Kv channels

We have interpreted published site-directed (Table 1) and cysteine-scanning (Table 2) mutagenesis data on Kv channels in terms of restraints on possible models. In both tables we summarize the published data for each residue in the H5 region from Pro<sup>1</sup> to Pro<sup>21</sup>. We have qualified mutagenesis data either as an orientational restraint, i.e., data that support the exposure of a residue to the channel lumen, or as a topological restraint, i.e., supporting the location of a residue at the intra- versus extracellular mouth of the Kv channel pore.

To indicate the manner in which these data have been interpreted, let us take a single residue, Val<sup>14</sup>, as an example. Val<sup>14</sup> immediately precedes the characteristic GYG motif of Kv channels. In a study of the residues of the Kv channel "signature sequence" comprising the eight residues TMTTVGYG in *Shaker*, replacement of Val<sup>14</sup> by Ala, Gly, Asn, or Gln resulted in loss of selectivity for potassium over sodium, whereas three other substitutions (Cys, Leu, and Thr) retained normal selectivity (Heginbotham et al., 1994). A number of studies involving a chimeric channel in which the H5 region of Kv2.1 was substituted for the H5 region of

**TABLE 1 Site-directed mutagenesis of Kv channel H5 region**

Equivalent residue in <i>Shaker</i> -H5	Mutant	Effect	Restraint	Reference
Pro <sup>1</sup>	—	—	—	
Asp <sup>2</sup>	Sh D431K	Effected block by externally applied TEA	E, P	(MacKinnon and Yellen, 1990)
	Sh D431	Direct effect on CTX block	P	(Pescobar et al., 1993)
	Kv2.1/Kv3.1 D372X	Contributes to CTX site	E, P	(MacKinnon and Miller, 1989) (Gross et al., 1994)
Ala <sup>3</sup>	—	—	—	
Phe <sup>4</sup>	Sh F433Y/S	Small effect on selectivity	P?	(Yool and Schwarz, 1991)
Trp <sup>5</sup>	—	—	—	
Trp <sup>6</sup>	—	—	—	
Ala <sup>7</sup>	—	—	—	
Val <sup>8</sup>	—	—	—	
Val <sup>9</sup>	Kv3.1/Kv2.1 V369L	altered $G_{Rb+}$ from Kv3.1 to Kv2.1	P	(DeBiasi et al., 1993)
Thr <sup>10</sup>	Sh T439G,S	S mutation reduced selectivity, $G_{nonselective}$	P	(Heginbotham et al., 1994)
Met <sup>11</sup>	Sh M440I	TEA <sub>INT</sub> binding drastically reduced	P, I	(Choi et al., 1993)
Thr <sup>12</sup>	Sh T441S	TEA <sub>INT</sub> binding reduced	I, P	(Yellen et al., 1991)
	Sh T441S	$G_{NH4+}$ increased	P	(Yool and Schwarz, 1991)
	Sh T441S	Effected block by internal hydroxylamine	I, P	(Yool and Schwarz, 1995)
Thr <sup>13</sup>	Sh T442S	N-type inactivation decreased	I	(Yool and Schwarz, 1995)
Val <sup>14</sup>	Sh V443X	Effected selectivity	P	(Heginbotham et al., 1994)
	Sh/Kv3.1 V443L	Switched $G_{K+}$ , TEA <sub>INT</sub> , Ba <sup>2+</sup> block and	P?	(Kirsch et al., 1992)
	Kv3.1/Kv2.1 V374L	$G_{Rb+}$ from Kv3.1 to Kv2.1 values	I, P	(Taglialatela et al., 1993) (Taglialatela et al., 1993) (Taglialatela et al., 1992) (Aiyar et al., 1994) (Harris and Isacoff, 1996)
	Kv3.1/Kv1.3 V398L	TEA <sub>INT</sub> altered to Kv1.3 like values Mg <sup>2+</sup> blocking kinetics reduced. Electrical distance suggested a deep-pore location	P, halfway	
	Kv3.1 L401V			
Gly <sup>15</sup>	Sh G444X	Nonselective channels	P	(Heginbotham et al., 1994)
Tyr <sup>16</sup>	Sh Y445V	Reduced selectivity	P	(Heginbotham et al., 1994)
	Sh $\Delta$ 445	Loss of selectivity	P	(Heginbotham et al., 1992)
Gly <sup>17</sup>	Sh G446X	Nonselective channels	P	(Heginbotham et al., 1994)
	Sh $\Delta$ 447	Loss of selectivity	P	(Heginbotham et al., 1992)
Asp <sup>18</sup>	Kv2.1 D378T	Selectivity reduced, rectification altered	P	(Kirsch et al., 1995)
Met <sup>19</sup>	Kv2.1/Kv3.1 M389X	CTX sensitivity conferred by Met <sup>19</sup> (and also D2 see above).	E, P	(Gross et al., 1994)
Thr <sup>20</sup>	Kv1.3 H401Y	Effected block by externally applied TEA	E, P	(Busch et al., 1991)
	Sh T449K	Effected block by externally applied TEA	E, P	(MacKinnon and Yellen, 1990)
	Sh/Kv3.1 T449Y	TEA <sub>EXT</sub> and $G_{Rb+}$ switch from Sh to NGK2	E, P	
	Kv1.4 K533Y	TEA <sub>EXT</sub> and $K_{EXT}^+$ sensitivity effected	E, P	(Taglialatela et al., 1994)
	Kv1.4 K533Y	TEA <sub>EXT</sub> and $K_{EXT}^+$ sensitivity effected	E, P	(Pardo et al., 1992)
	Sh T449Y or F	Fourfold contribution of T449 to external TEA site	E, P	(Ludewig et al., 1993)
	Sh T449	Direct contribution to CTX binding	E	(Heginbotham and MacKinnon, 1992)
	Sh T449C	High susceptibility to Cd <sup>2+</sup> /Zn <sup>2+</sup> block	P	(MacKinnon et al., 1990) (Escobar et al., 1993) (Yellen et al., 1994)
Pro <sup>21</sup>				

Notes: Sh, *Shaker*, other channel nomenclature from Gutman and Chandy (1993); mutations are denoted as follows: T449Y indicates that residue Thr<sup>449</sup> was replaced by tyrosine, etc. X denotes more than one mutation made at that residue. Effect abbreviations: TEA<sub>INT/EXT</sub>, Tetraethylammonium, applied from the intra- or extracellular mouth of the channel;  $G_{ion}$ , conductance of ion (K, NH<sub>4</sub><sup>+</sup>, or Rb); CTX, charybdotoxin. Restraints abbreviations as follows: E, Extracellular mouth; I, intracellular mouth; P, exposed to the channel lumen (pore-lining); NP, not exposed to channel lining. A question mark (e.g., for Phe<sup>4</sup>) indicates a degree of uncertainty in assignment of a restraint.

**TABLE 2 Cysteine-scanning mutagenesis of Kv channel H5 region**

Equivalent residue in <i>Shaker</i> -H5	Ag <sup>+</sup> probed <i>Shaker</i> (Lü and Miller, 1995).	MTSET probed Kv2.1 (Kürz et al., 1995).	MTSET probed Kv2.1 (Pascual et al., 1995).	Suggested restraint	P <sub>i</sub>
Pro <sup>1</sup>	Exposed	MTSET external	Not tested	P, E	1
Asp <sup>2</sup>	Exposed	Not exposed	Not tested	P?	2
Ala <sup>3</sup>	Rarely exposed	Not exposed	Not tested	P?	0
Phe <sup>4</sup>	Buried	Not exposed	Not tested	NP	0
Trp <sup>5</sup>	Exposed	Nonfunctional	Not tested	P	1
Trp <sup>6</sup>	Exposed	Nonfunctional	Not tested	P	1
Ala <sup>7</sup>	Buried	Not exposed	Not tested	P?	-1
Val <sup>8</sup>	Buried	Not exposed	Not tested	P?	-1
Val <sup>9</sup>	Exposed	Not exposed	Not exposed	P?	2
Thr <sup>10</sup>	Not determined	Nonfunctional	MTSET internal	I	1
Met <sup>11</sup>	Not determined	Nonfunctional	MTSET internal	I	0
Thr <sup>12</sup>	Not determined	Not exposed	MTSET internal	I	1
Thr <sup>13</sup>	Not determined	Nonfunctional	MTSET internal	I	0
Val <sup>14</sup>	Exposed	Nonfunctional	MTSET internal	P, I	2
Gly <sup>15</sup>	Nonfunctional	Nonfunctional	Not exposed	NP?	0
Tyr <sup>16</sup>	Exposed	Nonfunctional	Not exposed	P	2
Gly <sup>17</sup>	Buried	Nonfunctional	Not exposed	NP	0
Asp <sup>18</sup>	Exposed	Nonfunctional	MTSET external	P, E	2
Met <sup>19</sup>	Exposed	MTSET external	MTSET external	P, E	2
Thr <sup>20</sup>	Exposed	MTSET external	MTSET external	P, E	2
Pro <sup>21</sup>	Exposed	Nonfunctional	Not exposed	P, NP?	1

Notes: Residue "exposures" are taken from the referenced publications. MTSET, (2-trimethylammoniummethyl)methanethiosulfonate bromide. MTSET is assumed to provide topological information only. Abbreviations as follows: E, Extracellular mouth; I, intracellular mouth; P, exposed to the channel lumen (pore-lining); NP, not pore-lining; P<sub>i</sub>, residue exposure index. See text for details.

Kv3.1 indicated that Val<sup>14</sup> was the primary determinant of the differences in internal TEA block and the conductance ratio  $G_K^+/G_{Rb^+}$  between Kv2.1 and Kv3.1 (Kirsch et al., 1992; Taglialatela et al., 1992, 1993a,b), and the same residue was identified as being partly responsible for the different sensitivity to internal TEA displayed between Kv3.1 and Kv1.3 (Aiyar et al., 1994). Additionally, the effect of residue 14 upon channel block by internal Mg<sup>2+</sup> was investigated by Harris and Isacoff (1996). They determined that the faster blocking kinetics of Kv3.1 (compared to *Shaker*) was due to the presence of Val at position 14 in *Shaker*-H5, compared to Leu at this position in Kv3.1. Substitution of Leu at this position into either channel produced fast blocking, whereas Val at position 14 in either channel produced slower block (Harris and Isacoff, 1996). Taken together, these results are consistent with residue 14 being exposed to the channel lumen, in a location close to the intracellular pore mouth. Recent electrical distance estimates suggest a deep-pore location (Harris and Isacoff, 1996). The results are reinforced by cysteine-scanning mutagenesis experiments (Table 2), which demonstrate that Cys<sup>14</sup> (i.e., Val<sup>14</sup> being mutated to Cys) is accessible both to Ag<sup>+</sup> ions (Lü and Miller, 1995) and to internally applied methanethiosulfonate reagents (Pascual et al., 1995), and suggest that Val<sup>14</sup> is oriented toward the channel lumen and is closer to the internal mouth than the external mouth of the channel. This is denoted by the P (pore-lining) and I (intracellular) in the "restraint" column of Tables 1 and 2.

Similar interpretations for other positions were used to label each residue in H5 with a Positional Index (P<sub>i</sub>) (Table 2) as follows:

- 1: Residue appears not to be exposed to the pore
  - 0: Conflicting data, or no available data
  - +1: Residue appears to be exposed to the pore by either Cys-scanning mutagenesis or by site-directed mutagenesis data
  - +2: Residue is identified as pore-lining by both site-directed mutagenesis and Cys-scanning mutagenesis
- In the absence of high-resolution three-dimensional structural data for the pore-lining region of Kv channels, there are two secondary structural motifs that can be investigated as possible models for the H5 region, namely an eight-stranded  $\beta$ -barrel and an eight-staved  $\alpha$ -helix bundle. Models for both structural classes are produced and described below.

### Mutagenesis defines 42 possible configurations of $\beta$ -barrel

If a  $\beta$ -barrel topology for the H5 region is assumed, there are still a number of variables that must be accounted for that would give rise to different final models. These parameters include the shear number and orientation (described below), but also the thread of H5 onto an idealized  $\beta$ -hairpin, i.e., the position of the loop within the sequence and the length of the  $\beta$ -strands. The thread thus determines which residues will line the pore of the resultant models. Candidate threads were examined by threading the H5 sequence onto idealized  $\beta$ -hairpin templates differing in the number of residues in the "downward" (N1) and "upward" (N2) strands, and in the position and number of residues in the

loop region (N3). N1 and N2 were varied from 6 to 11 residues, whereas N3 was varied from 2 to 4 residues. Thus each thread is identified by a numerical code N1-N3-N2. Threads were scored on a residue-by-residue basis by their agreement with the mutagenesis data interpreted as described above. At each position in the thread, a score was defined as the sum of the following components:

- +1 if the orientation of the residue agreed with mutagenesis
- +1 if the topology of the residue agreed with mutagenesis
- 0 if no data were available or if agreement was ambiguous
- 1 if the orientation of the residue disagreed with mutagenesis
- 1 if the topology of the residue disagreed with mutagenesis

Loop residues were excluded from the orientational score, as a residue within the loop would clearly expose its side chain to the ion conduction pathway. For similar reasons, the N- and C-terminal proline residues were excluded from the scoring. The score for a particular topology is summed over all residues. Sequence threading of H5 to idealized  $\beta$ -hairpins identifies four threads with the highest scores (Fig. 1). The four selected threads have scores of +12, +13, +8, and +10, respectively, for Fig. 1, A-D, and the overall range of scores is from -3 to +13. Clearly, none of these four idealized  $\beta$ -threads shows perfect agreement with mutagenesis data. In particular, none can have the pattern of pore-lining and non-pore-lining residues in the descending strand required for perfect agreement.

In addition to these four identified threads, there are three additional templates that require consideration. Although they are similar to three of the threads above, they have different hydrogen bond requirements and so should be considered as distinct. The 8-3-9, 7-4-9, and 9-4-7 threads usually would have a pair of hydrogen bonds between the residues immediately preceding and following the loop and would form 3:3 and 4:4  $\beta$ -hairpins (Sibanda et al., 1989). However, so-called 3:5 and 4:6  $\beta$ -hairpins do not have these hydrogen bonds and thus form a somewhat looser turn (Sibanda et al., 1989). Threads in which hydrogen bonds are not required immediately adjacent to the loops are denoted with the letter *L* (Loose).

A  $\beta$ -barrel configuration for the H5 region may be thus defined in terms of three parameters. These are:

1. The thread (discussed above)
2. The shear number of the barrel. The shear number (*S*) of a  $\beta$ -barrel is a measure of the angle between the component strands and the central barrel axis. Here we define *S* as the number of residues moved along a strand *A* by following the hydrogen-bonding pattern from residue *j* on strand *A* around the barrel until strand *A* is reached again (strand *A'* in Fig. 2). In this nomenclature a stable eight-stranded  $\beta$ -barrel can adopt a shear number of 8, 10, or 12 (Murzin et al., 1994; Sansom and Kerr, 1995).

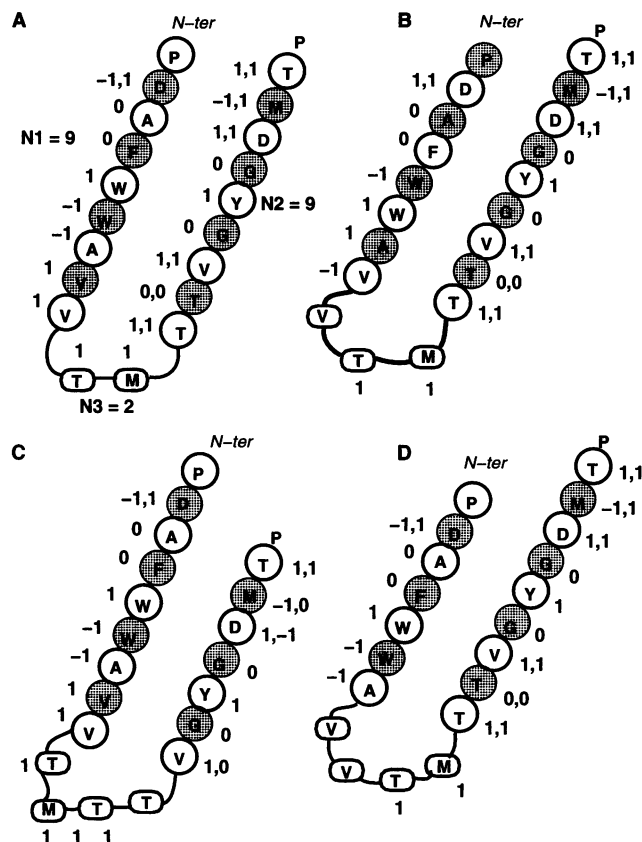


FIGURE 1 Threading of *Shaker*-H5 to idealized  $\beta$ -hairpins. H5 was threaded onto ideal  $\beta$ -hairpins as described in the text. Shown here are the four highest scoring threads. The four threads are identified by the numerical codes (A) 9-2-9, (B) 8-3-9, (C) 7-4-9, and (D) 9-4-7 (i.e., 9-2-9 is a hairpin where each strand is nine residues in length, with a two-residue loop at residues 10 and 11 (Thr-Met)). Pore-lining residues are represented by open circles; shaded circles represent non-pore-lining residues. Loop residues are boxed. Scores for each residue are given. Where there is both an orientational restraint and a topological restraint for a particular residue, the score against the orientational data is given first, i.e., for residue D2 in thread 9-2-9 (A), the residue disagrees with its orientational restraint (scores -1), but agrees with its topological restraint (scores +1). The total scores for the four threads are (A) +12, (B) +13, (C) +8, (D) +10.

3. The orientation of the component strands around the barrel axis. The orientation of strands around the barrel when viewed from the extracellular face can be either anticlockwise (A) or clockwise (C) (Fig. 2).

Thus, as defined above, there are seven possible threads (9-2-9, 8-3-9, 9-4-7, 7-4-9, 8-3-9-L, 7-4-9-L, and 9-4-7-L), three shear numbers ( $S = 8$ ,  $S = 10$ , and  $S = 12$ ), and two orientations (anticlockwise and clockwise) that must be considered. This combinatorial definition of  $\beta$ -barrels leads to  $7 \times 3 \times 2 = 42$  possible configurations of  $\beta$ -barrel to be explored. Our nomenclature for these configurations is "shear-thread orientation" (i.e., the configuration S10-839-LA has a shear number of 10, a thread 8-3-9 with no hydrogen bonds adjacent to the loop residues, and a anticlockwise orientation of strands around the barrel axis). This nomenclature is simpler than that employed in a pre-

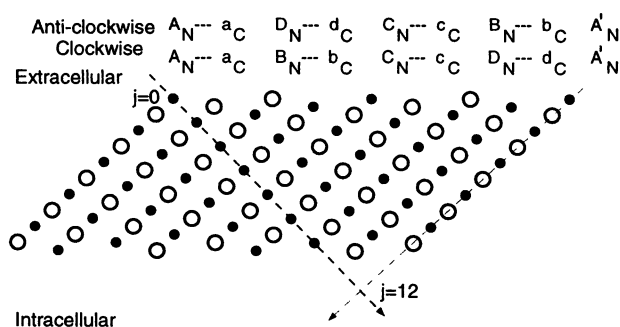


FIGURE 2 Structural features of  $\beta$ -barrels. An eight-stranded  $\beta$ -barrel is represented by a 2D projection of the  $C\alpha$  atoms, such that filled circles represent pore-lining residues and open circles represent residues facing the exterior. Subscripts N and C denote the N- and C-termini of H5. The strand at the far right (i.e.,  $A'$ ) is the same as the first strand. The shear number of the barrel ( $S$ ), a measure of the angle between each strand and the central barrel axis, is identified by following the hydrogen-bonding pattern around the barrel circumference from residue  $j = 0$  of the first strand to residue  $j = S$  of strand  $A'$ . Thus, in this case,  $S = 12$ . Possible orientations of H5 around the barrel axis (clockwise and anticlockwise) are also indicated.

vious analysis of  $\beta$ -barrel models of the Kv channel pore (Bogusz et al., 1992), although that study had an invariant shear number ( $S = 8$ ). For example, the configuration here termed S8-839-LA would correspond to a configuration T439 CCW 3:5 in the nomenclature of Busath and colleagues (Bogusz et al., 1992).

### Unique combinations of restraints files define each $\beta$ -barrel configuration

For each of the 42 different configurations described above, a unique combination of restraints files was required in DG/SA structure generation and SA/MD refinement to generate ensembles of candidate structures:

1. Dihedral angle restraints. Torsion angle restraints on the  $\phi$  and  $\psi$  angles of those residues in a  $\beta$ -strand conformation define the thread of a configuration. Target values are  $\phi = -135 (\pm 30^\circ)$ ,  $\psi = +135 (\pm 30^\circ)$ . For configurations with relaxed hydrogen-bond requirements proximal to the loop (i.e., L-configurations), the allowed deviations on  $\phi$ ,  $\psi$  of residues adjacent to the turn were increased to  $\pm 50^\circ$ .

2. Intrahairpin hydrogen bond restraints. Distance restraints, acting between O atoms and H atoms of residues in the same H5 segment, are unique for the thread of a configuration. Target hydrogen bond distances were  $1.92 \pm 0.15 \text{ \AA}$  (Baker and Hubbard, 1984). For configurations with relaxed hydrogen-bond requirements proximal to the loop (i.e., L-configurations), the restraints involving residues adjacent to the turn were removed (Sibanda et al., 1989).

3. Interhairpin hydrogen bond restraints. Distance restraints, acting between O atoms and H atoms of residues in adjacent H5 segments, describe the orientation and shear number of the  $\beta$ -barrel. Again, target distances were  $1.92 \pm 0.15 \text{ \AA}$  (Baker and Hubbard, 1984).

4. Cross-pore distance restraints. Distance restraints acting between  $C\beta$  atoms of equivalent pore-lining residues on opposite sites of the pore reflect the shear number, and were determined from ensembles of idealized eight-stranded Ala<sup>10</sup>  $\beta$ -barrels (Sansom and Kerr, 1995) with shear numbers  $S = 8$ ,  $S = 10$ , and  $S = 12$ . The target distances were  $10.2 \text{ \AA}$ ,  $11.0 \text{ \AA}$ , and  $11.7 \text{ \AA}$ , respectively.

### $\beta$ -Barrel modeling by DG/SA and SA/MD

Of the 42 configurations, two, S10-749-A and S10-947-LA, failed to yield any structures after DG/SA. This indicates that no solutions to the restraints files for these two ensembles with the correct  $\beta$ -strand chirality were possible. The other 40 configurations yielded between 2 and 100 structures (Table 3). The degree of structural variation within an ensemble and the structural consequences of different shear numbers are evident in Fig. 3. Before side-chain addition of the DG/SA produced structures, the members of each ensemble were ranked. Structures 1 were ranked according to a number of criteria: 1) the number of violations of input dihedral angle and distance restraints ( $v_i$ ), 2) the backbone stereochemistry of the models ( $b_i$ ), assessed by the number of residues in the disallowed region of the Ramachandran plot as defined by Procheck (Morris et al., 1992), 3) the fourfold symmetry of the model ( $r_i$ ; defined in Kerr et al., 1994), and 4) the energy of the model ( $u_i$ ). A normalized score ( $T_i$ ) for each structure was calculated as follows:

$$T_i = 1 - \frac{(v_i/V) + (b_i/B) + (r_i/R) + (u_i/U)}{4}$$

where  $V$ ,  $B$ ,  $U$ , and  $R$  are the mean values of  $v$ ,  $b$ ,  $u$ ,  $r$  averaged across all 2784 models in all 40 ensembles. Thus a  $T_i$  value of 0 indicates an "average" structure compared against all structures in all 40 ensembles. Values for  $T_i$  across all members of all ensembles are presented in Table 3. There is also considerable variation in the value of  $T_i$  for individual structures within an ensemble. Fig. 4 indicates typical distributions of  $T_i$  observed across four ensembles that share the same thread (9-4-7) and shear number ( $S = 8$ ), but differ in terms of orientation and hydrogen-bond restraints proximal to the turn. The observed large variation in  $T_i$  across ensembles gives rise to  $\langle T_i \rangle$  values greater than 0 for most ensembles. At this stage it is possible to tentatively suggest which threads yield less plausible models of Kv channel pores. In particular threads 7-4-9 and 9-4-7 yield fewer structures with  $T_i < 0$  (and their mean  $T_i$  scores are also higher) than 9-2-9 and 8-3-9 threads. However, a more complete ranking of the models was only possible once they had been refined by the addition of side chains.

Five structures selected from each DG/SA-generated ensemble were refined by simulated annealing via restrained molecular dynamics (SA/MD) (Kerr et al., 1994) to add side chain atoms of the H5 sequence to the restrained backbone (see Methods). Structures were selected at random from those members of each ensemble that had  $T_i < 0$ . Where

**TABLE 3** Scoring of DG/SA generated  $\beta$ -barrel ensembles

Configuration	$N_{DG}$	$\langle T_i \rangle$	$\%T_i < 0$	$T_{i(MIN)}$
S8-929-A	51	0.16 (0.68)	49	-0.84
S8-929-C	42	0.10 (0.86)	64	-0.86
S10-929-A	96	0.42 (0.88)	40	-0.72
S10-929-C	99	0.43 (0.97)	43	-0.70
S12-929-A	83	0.18 (0.72)	57	-0.69
S12-929-C	83	0.17 (0.74)	55	-0.70
S8-947-A	51	0.27 (0.48)	27	-0.48
S8-947-C	43	0.66 (0.81)	16	-0.12
S8-947-LA	54	0.43 (0.53)	19	-0.45
S8-947-LC	49	0.30 (0.55)	31	-0.60
S10-947-A	76	0.75 (0.78)	12	-0.32
S10-947-C	32	1.25 (0.63)	0	+0.32
S10-947-LC	98	0.71 (0.62)	10	-0.49
S12-947-A	100	0.70 (0.63)	17	-0.22
S12-947-C	100	0.75 (0.71)	10	-0.23
S12-947-LA	99	0.72 (0.63)	7	-0.36
S12-947-LC	100	0.53 (0.47)	11	-0.35
S8-749-A	54	0.38 (0.61)	31	-0.47
S8-749-C	53	0.43 (0.59)	28	-0.20
S8-749-LA	47	0.48 (0.66)	47	-0.54
S8-749-LC	52	0.57 (0.76)	19	-0.32
S10-749-C	50	0.68 (0.75)	6	-0.24
S10-749-LA	7	0.95 (0.38)	0	+0.33
S10-749-LC	100	0.76 (0.61)	5	-0.42
S12-749-A	100	0.57 (0.72)	26	-0.58
S12-749-C	100	0.60 (0.69)	17	-0.52
S12-749-LA	100	0.85 (0.86)	2	-0.16
S12-749-LC	100	0.86 (0.54)	4	-0.24
S8-839-A	59	0.32 (0.62)	41	-0.57
S8-839-C	54	0.25 (0.76)	52	-0.78
S8-839-LA	53	0.00 (0.61)	64	-0.86
S8-839-LC	60	0.16 (0.52)	43	-0.69
S10-839-A	5	0.59 (0.61)	40	-0.16
S10-839-C	35	0.55 (0.81)	26	-0.49
S10-839-LA	2	-0.09 (0.41)	50	-0.50
S10-839-LC	97	0.38 (0.68)	32	-0.53
S12-839-A	100	0.44 (0.58)	31	-0.50
S12-839-C	100	0.53 (0.70)	31	-0.61
S12-839-LA	100	0.43 (0.71)	32	-0.61
S12-839-LC	100	0.19 (0.56)	47	-0.70

$N_{DG}$ , Number of structures produced by distance geometry and simulated annealing;  $\langle T_i \rangle$ , mean ( $\pm$ SD) score across DG/SA ensemble (see text);  $\%T_i < 0$ , percentage of structures in DG/SA ensemble with  $T_i < 0$ ;  $T_{i(MIN)}$ , lowest  $T_i$  within the ensemble. Ensembles S10-947-LA and S10-749-A produced no structures in DG/SA and are thus excluded from this table.

fewer than five members on an ensemble had  $T_i < 0$ , the highest ranking five structures were refined. For each of the selected structures, independent runs of stage 1 ( $m = 2$ ) and stage 2 ( $n = 2$ ) generated ensembles of  $5 \times 2 \times 2 = 20$  structures for each configuration. A total of 779 structures were produced across the 40 ensembles by SA/MD. The analysis of these models is discussed below.

### Twenty-four configurations of $\alpha$ -helix bundle can be defined

The second structural motif that could underlie the pore region of the Kv channel is an  $\alpha$ -helix bundle. In these

configurations, each H5 segment would form an  $\alpha$ -helical hairpin, thus generating an eight-staved  $\alpha$ -helix bundle. As with  $\beta$ -barrel geometry, there are a number of variables defining distinct  $\alpha$ -helix bundle configurations (Fig. 5):

1. The position of the loop within the H5 sequence
2. The length of the loop
3. The overall orientation of helices when viewed from the extracellular face (i.e., clockwise or anticlockwise)
4. The orientation of the two helices of a helical-hairpin ( $\theta_1$  and  $\theta_2$ ), which determine which residues will point toward the center of the resulting eight-helix bundle
5. The crossing angle between adjacent helices,  $\Omega$

Parameters 1, 2, and 3 define the "thread" of the  $\alpha$ -helix bundle. Threads were considered with either two-, three-, or four-residue turns, in which the loop was entirely within the seven-residue sequence from Val<sup>8</sup> to Val<sup>14</sup>. These limits were chosen so that each  $\alpha$ -helix would contain at least seven residues (i.e., two complete  $\alpha$ -helical turns). Twenty-four possible configurations are thus defined (listed in Table 5). Each thread is identified by the number of residues in the turn (T), the residue preceding the turn, and the orientation of the overall helix bundle. Thus the code T3-Thr10-C describes a configuration with a three-residue turn comprising residues Met<sup>11</sup> to Thr<sup>13</sup>, with helices arranged clockwise when viewed from the extracellular face. For each thread the optimal combination of ( $\theta_1$ ,  $\theta_2$ ,  $\Omega$ ) was determined by a grid search.  $C\alpha$  templates were generated on a grid with  $\theta_1 = 0$  to  $360^\circ$ ,  $\theta_2 = 0$  to  $360^\circ$ , and  $\Omega = -20$  to  $+20^\circ$ , using  $4^\circ$  intervals for each parameter. Each eight-helix bundle template (containing only  $C\alpha$  atoms) was scored for its agreement with the restraints derived from the site-directed and cysteine-scanning mutagenesis data as follows: for each residue  $i$ , a cross-pore distance  $R_{1-3}$  was calculated between  $C\alpha-i$  on the first H5 helical-hairpin and  $C\alpha-i$  on the third (i.e., opposite) H5 helical-hairpin. For residues that are suggested to be pore-lining (Tables 1 and 2), we score  $A_i$ , where

$$A_i = R_{1-3} - 22$$

whereas for residues that are suggested to be non-pore-lining, we score

$$A_i = 28 - R_{1-3}$$

The values of 22 Å and 28 Å are obtained from analysis of the cross-pore  $C\alpha$  distances of idealized eight-helix bundles (Kerr, unpublished observations). Thus the score for each ( $\theta_1$ ,  $\theta_2$ ,  $\Omega$ ) combination is summed over all residues,  $\Sigma A_i$ . Thus a ( $\theta_1$ ,  $\theta_2$ ,  $\Omega$ ) combination that has  $C\alpha$  atoms oriented in agreement with the mutagenesis data will have a low  $\Sigma A_i$  and vice versa. The range of  $\Sigma A_i$  values was between 15 and 60. Fig. 6 displays the variation in  $\Sigma A_i$  as a function of ( $\theta_1$ ,  $\theta_2$ ) for a fixed value of  $\Omega$  for the thread T3-Thr10-A. It is clear that the global minimum occurs at  $\theta_1 = 190^\circ$ ,  $\theta_2 = 180^\circ$ , and there is a local minimum at  $\theta_2 = 300^\circ$ . The global minimum in ( $\theta_1$ ,  $\theta_2$ ,  $\Omega$ ) was employed as the starting  $C\alpha$  model for SA/MD.

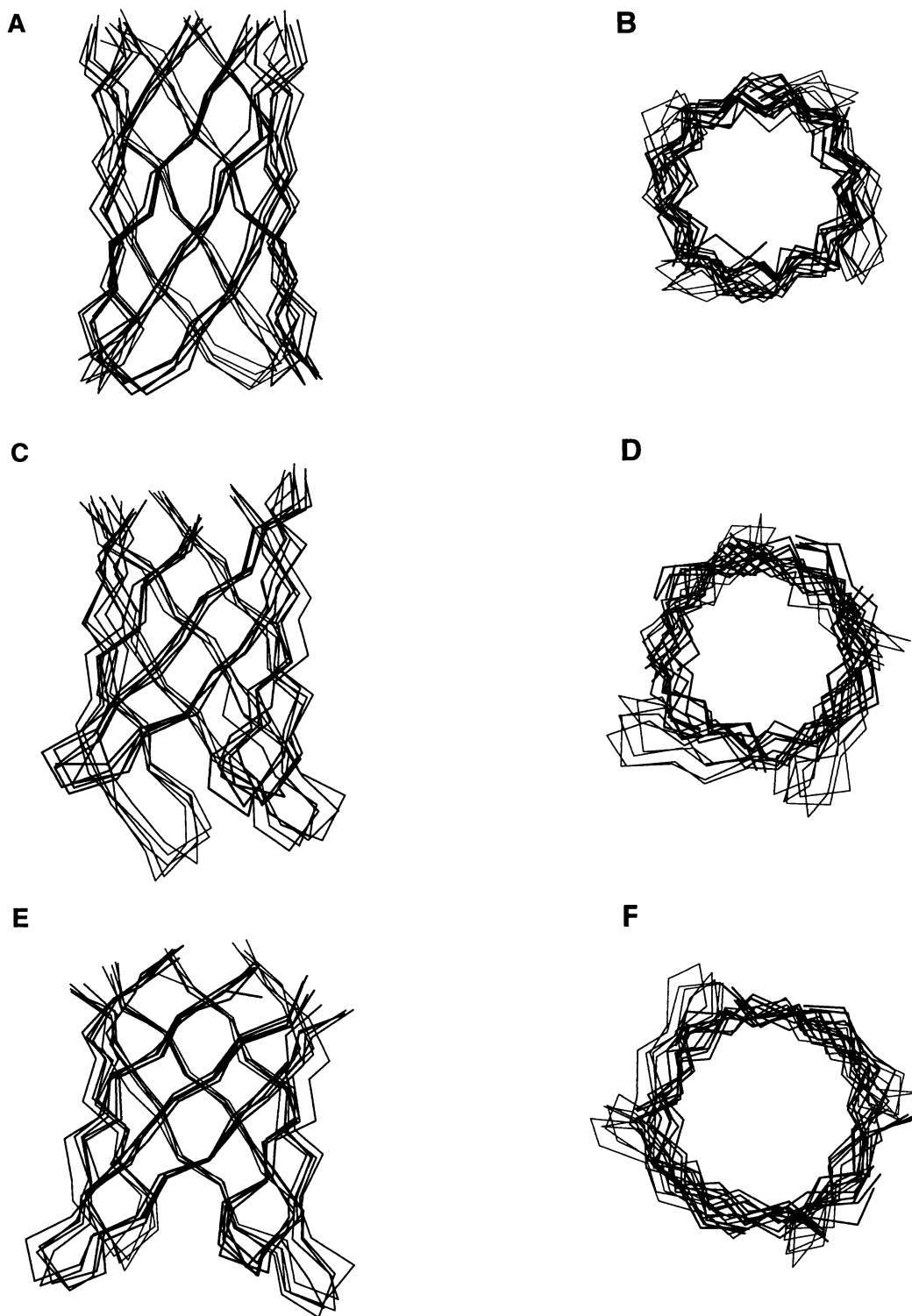


FIGURE 3 Distance geometry-generated ensembles. Five structures from the ensembles S8-929-C (A, B), S10-929-C (C, D), and S12-929-C (E, F) are shown as superimposed  $C\alpha$  traces. A, C, and E are parallel to the channel axis with the extracellular face uppermost, and B, D, and F are looking along the pore axis from the extracellular mouth. The increasing shear number is visible as an increase in the tilt of strands to the channel axis (A, C, E) and a shorter but wider pore.

Ensembles of  $\alpha$ -helix bundle structures were generated from  $C\alpha$  templates by simulated annealing via restrained molecular dynamics (Kerr et al., 1994). During SA/MD,

$\alpha$ -helicity, and thus the thread, was maintained by distance restraints between the O atom of residue  $i$  and the H atom of residue  $i + 4$ . A single distance restraint acted between

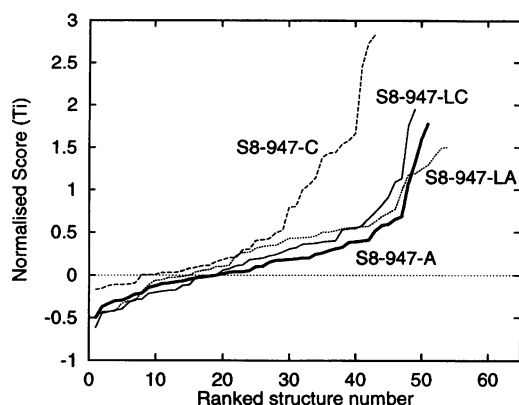


FIGURE 4 Ranking of distance geometry-generated ensembles. The normalized score (see text) is plotted for four ensembles, sharing a common thread and shear number. For each ensemble, between 40 and 55 structures were generated by distance geometry and simulated annealing. Structures satisfying most of the input dihedral angle and distance restraints, while maintaining good stereochemistry and high symmetry, have  $T_i$  values less than 0. Thus the S8-947-C ensemble has seven structures with  $T_i < 0$ , whereas the other three S8-947 ensembles have  $\sim 15$ – $20$ . Five structures with  $T_i < 20$  are selected for side-chain addition and further refinement.

neighboring  $\alpha$ -helices, and there were no distance restraints across the pore lumen. For each  $C\alpha$  template, independent runs of stage 1 ( $m = 6$ ) and stage 2 ( $n = 4$ ) generated ensembles of  $6 \times 4 = 24$  structures for each configuration. The variation across an  $\alpha$ -helical ensemble is evident in Fig. 7, which represents the entire T2-Thr10-A ensemble as a ribbon diagram. Although there are some highly symmetrical structures (for example, the structure indicated by an *asterisk*), there are also many structures in which some helices become almost perpendicular to the channel axis (for example, marked by a # in Fig. 7).

#### Analysis of $\beta$ -barrel and $\alpha$ -helix bundle models of (H5)<sub>4</sub>

The modeling procedures described have given rise to 64 ensembles of models for the pore-lining H5 region of Kv channels, 40 with an eight-stranded  $\beta$ -barrel architecture, and 24 with an eight-helix bundle. The total number of models is 1355, comprising 779  $\beta$ -barrel models and 576  $\alpha$ -helix bundle models. To identify candidate models for further refinement studies, it is necessary to compare the ensembles and rank them.

Ensembles could not be ranked by evaluation of their energies. There is virtually no difference in the mean total potential energy of the ensembles (data not shown). The interaction energy (i.e., the nonbonded energy between adjacent H5 segments, which stabilizes the H5 tetramer) is considerably more favorable for  $\beta$ -barrels than  $\alpha$ -helix bundles (not shown), reflecting the hydrogen-bond network that defines the  $\beta$ -barrel. However, interaction energies could not be employed to rank within the  $\alpha$ -helical or  $\beta$ -barrel configurations.

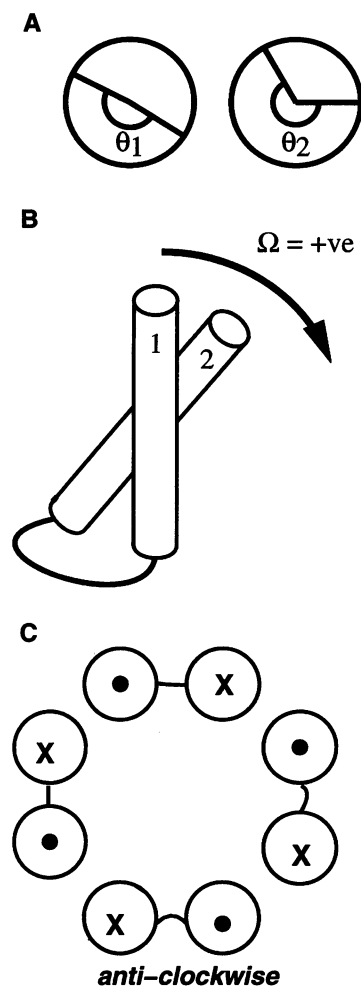


FIGURE 5 Construction of initial  $\alpha$ -helix bundle ensembles. The H5 unit is represented as an  $\alpha$ -helical hairpin. Four parameters can be varied to generate alternative  $C\alpha$  templates for  $\alpha$ -helix bundles before simulated annealing via restrained molecular dynamics. The parameters are as follows: (A) The orientation of each helix in the hairpin about its long axis ( $\theta_1$ ,  $\theta_2$ ). Each helix is represented as a cylinder viewed looking down the long axis. (B) The crossing angle between adjacent helices ( $\Omega$ ). (C) The orientation of the overall helix bundle. Each helix is represented as a circle. A  $\odot$  corresponds to a helix pointing from the intracellular side to the extracellular side, and a  $\otimes$  corresponds to a helix pointing from the extracellular side to the intracellular side. Shown is the anticlockwise orientation viewed from the extracellular face.

As potential energy cannot be used to rank ensembles, we have analyzed a number of geometrical properties that may be useful in ranking configurations and present the data in Tables 4 and 5. The stereochemical quality of the peptide backbone ( $B$ ), a measure of the number of residues in the less favorable regions of the Ramachandran plot, indicates that the two-residue turns in  $\beta$ -barrels introduce some strain into the backbone at this point that is not seen for the four-residue turns (Table 4). In  $\alpha$ -helix bundle configurations, the length of turn is uncorrelated with  $B$ . It is clear that the  $\alpha$ -helix bundle configurations (Table 5) have a much higher degree of variation across an ensemble with RMSD values for backbone atoms between 2.7 Å and 3.6 Å,

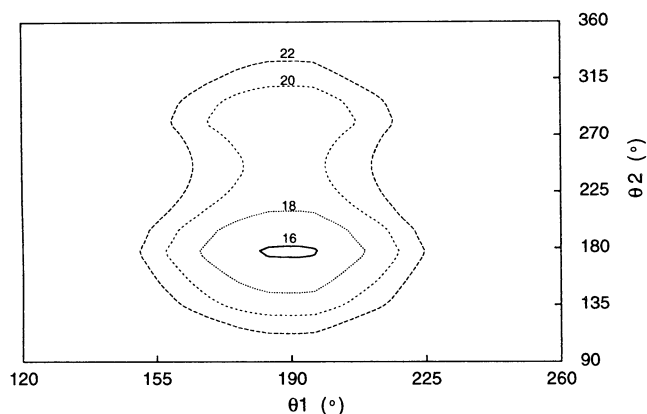


FIGURE 6 Scoring of initial  $\alpha$  templates. Combinations of  $(\theta_1, \theta_2, \Omega)$  were generated by grid searching, and each template was scored as described. Preferred combinations of  $(\theta_1, \theta_2, \Omega)$  for each thread are identified by contour plots. Displayed is a contour plot of score versus  $(\theta_1, \theta_2)$  for a constant value of  $\Omega = -12^\circ$  for the thread T3-Thr10. The solid line is the contour indicating the lowest score (i.e., preferred combination of  $(\theta_1, \theta_2)$ ,  $\Sigma A_i = 16$ ), while other contours reflect poorer agreement. The global minimum occurs at  $\theta_1 = 188^\circ$ ,  $\theta_2 = 178^\circ$ , and there is a local minimum at  $\theta_2 = 300^\circ$ . A combination of  $\theta_1 = 0^\circ$  and  $\theta_2 = 0^\circ$  orients the hairpins such that the pore-lining faces of the  $\alpha$ -helices are defined by residues Phe<sup>4</sup>, Ala<sup>7</sup>, and Gly<sup>15</sup>.

whereas  $\beta$ -barrel ensembles show less backbone variation with RMSD values between 0.9 Å and 1.8 Å. This reflects the presence of multiple restraints between adjacent  $\beta$ -strands (i.e., inter- and intrahairpin hydrogen-bond restraints). This also produces structures with a higher degree of fourfold symmetry (mean  $R_{\text{sym}}$  for  $\beta$ -barrel ensembles is 5.1 Å, compared to 8.8 Å for  $\alpha$ -helix bundle ensembles; Tables 4 and 5). It should be noted that we have not imposed symmetry during the modeling. Although Kv channels are homotetrameric proteins, there is no evidence that side-chain or loop conformations obey exact fourfold rotational symmetry. Such structural properties are, however, still insufficient for ranking ensembles, although they could be employed for ranking individual members of a particular ensemble (i.e., the structure with the highest degree of fourfold symmetry, combined with a stereochemically correct backbone). Instead, ranking by comparison of predicted and experimental pore properties was employed.

### Pore radius profiles and predicted conductance of Kv channel models

Predicted properties of the H5 models can be compared to experimentally obtained characteristics of Kv channels. Pore radius profiles were calculated for all members of all ensembles using the program HOLE (Smart et al., 1993). The results are presented in Tables 4 and 5 and in Figs. 8 and 9. Two trends are evident from these data. First is an increase in minimum pore radius with shear number for  $\beta$ -barrels, as is illustrated in Fig. 8. The  $S = 8$  configuration (Fig. 8, A and B) has a mean minimum pore radius across the ensemble of only  $0.50 \pm 0.18$  Å, which increases in the

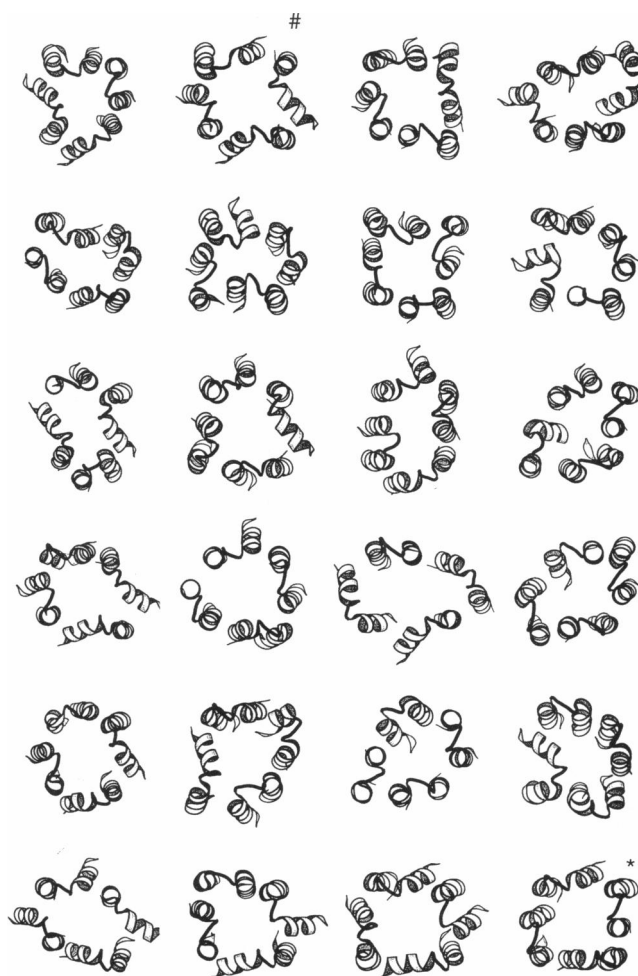


FIGURE 7 Ribbon representation of a T2-Thr10-A ensemble. Structures generated in stage 2 of SA/MD from the same stage 1 structure form the rows of the figure. The highlighted structures indicate a highly symmetrical structure (\*), and a structure in which component  $\alpha$ -helices become less perpendicular to the membrane plane (#).

$S = 10$  ensemble (Fig. 8, C and D) to  $0.80 \pm 0.42$  Å, and to  $1.15 \pm 0.45$  Å for the  $S = 12$  ensemble (Fig. 8, E and F). The second evident trend is the greater pore radius of  $\alpha$ -helix bundles compared to  $\beta$ -barrels. Indeed, all of the eight-helix bundle configurations have a higher minimum pore radius than the  $\beta$ -barrel ensembles. There is, however, considerable variation between the helix bundle ensembles in pore radius. Fig. 9 depicts three configurations with a low ( $1.71 \pm 0.85$  Å), medium ( $2.55 \pm 0.81$  Å), and high ( $3.26 \pm 1.28$  Å) minimum pore radius. It should be noted that the variation in pore radius within the  $\alpha$ -helix bundle ensembles is considerably greater (reflecting the higher RMSD of these ensembles), but also that the pore is considerably shorter. From Figs. 8 and 9 it can be seen that the narrow region of the pore extends for some 20–25 Å in  $\beta$ -barrel models, but for only 10–15 Å in  $\alpha$ -helix bundle ensembles. Although this may seem unlikely in the context of membrane-spanning pores (given that the thickness of the lipid bilayer is  $\sim 30$  Å), it should be remembered that the H5 region is in

**TABLE 4** Properties of  $\beta$ -barrel ensembles

Configuration	$N_{\text{refine}}$	$B$	$R_{\text{sym}}$ (Å)	$\text{RMSD}_b$ (Å)	$R_{\text{min}}$ (Å)	$G_{\text{pred}}$ (pS)	$M$
S8-929-A	20	16.0 (5.3)	2.8 (0.4)	0.93	0.57 (0.22)	2.5	-0.25
S8-929-C	20	13.6 (4.2)	2.6 (0.2)	0.89	0.52 (0.39)	2.5	-0.23
S10-929-A	20	11.8 (2.5)	5.3 (0.4)	0.93	0.50 (0.29)	1.9	-0.25
S10-929-C	20	12.4 (4.5)	5.2 (0.3)	0.88	0.63 (0.29)	3.5	-0.22
S12-929-A	19	12.0 (3.8)	5.3 (0.3)	0.96	0.83 (0.34)	4.8	-0.26
S12-929-C	20	10.0 (3.2)	5.4 (0.4)	0.89	0.65 (0.38)	4.0	-0.27
S8-947-A	20	10.3 (2.7)	4.4 (0.6)	1.5	0.53 (0.33)	2.1	-0.25
S8-947-C	20	8.7 (2.7)	4.3 (0.5)	1.3	0.54 (0.20)	2.4	-0.21
S8-947-LA	20	8.2 (3.4)	4.1 (0.8)	1.4	0.58 (0.17)	2.4	-0.22
S8-947-LC	20	6.7 (3.4)	3.9 (0.5)	1.4	0.54 (0.20)	2.4	-0.24
S10-947-A	20	8.9 (2.7)	5.9 (0.5)	1.4	0.76 (0.30)	3.3	-0.24
S10-947-C	20	9.4 (2.7)	7.0 (0.8)	1.8	0.72 (0.30)	3.5	-0.29
S10-947-LC	20	6.2 (2.8)	5.7 (0.5)	1.3	0.80 (0.42)	3.8	-0.24
S12-947-A	20	9.8 (2.8)	6.4 (0.4)	1.5	1.15 (0.45)	7.8	-0.24
S12-947-C	20	9.2 (2.2)	5.7 (0.6)	1.3	0.86 (0.44)	5.4	-0.23
S12-947-LA	20	9.5 (3.3)	6.1 (0.6)	1.5	0.97 (0.47)	6.3	-0.22
S12-947-LC	20	7.7 (3.6)	5.7 (0.5)	1.3	1.02 (0.33)	6.3	-0.22
S8-749-A	20	11.5 (0.36)	4.0 (0.6)	1.5	0.54 (0.34)	2.7	-0.09
S8-749-C	20	11.4 (3.5)	4.0 (0.5)	1.5	0.46 (0.39)	2.2	-0.06
S8-749-LA	20	9.0 (3.3)	4.2 (0.6)	1.6	0.55 (0.26)	2.8	-0.12
S8-749-LC	18	10.8 (4.7)	4.4 (0.8)	1.6	0.59 (0.23)	2.8	-0.09
S10-749-C	20	11.3 (3.6)	6.4 (0.4)	1.5	0.58 (0.32)	3.6	-0.11
S10-749-LA	20	15.4 (4.7)	7.0 (0.6)	1.8	0.72 (0.35)	4.5	-0.07
S10-749-LC	20	8.4 (3.9)	5.8 (0.5)	1.4	0.52 (0.28)	3.5	-0.10
S12-749-A	20	8.2 (5.1)	6.1 (0.5)	1.4	0.68 (0.25)	4.6	-0.10
S12-749-C	20	5.9 (3.5)	6.0 (0.6)	1.4	0.72 (0.24)	4.6	-0.14
S12-749-LA	20	12.3 (3.6)	6.6 (0.6)	1.7	0.75 (0.28)	5.2	-0.07
S12-749-LC	20	6.2 (3.2)	6.2 (0.5)	1.5	0.85 (0.31)	5.6	-0.10
S8-839-A	18	12.3 (3.3)	3.0 (0.4)	1.1	0.60 (0.33)	2.1	-0.32
S8-839-C	20	12.8 (4.4)	3.0 (0.5)	1.0	0.42 (0.18)	1.8	-0.36
S8-839-LA	20	13.1 (5.1)	3.3 (0.4)	1.1	0.58 (0.22)	2.2	-0.40
S8-838-LC	17	14.0 (5.4)	3.2 (0.6)	1.2	0.50 (0.18)	1.9	-0.34
S10-839-A	20	12.5 (4.1)	5.6 (0.6)	1.2	0.56 (0.25)	2.6	-0.36
S10-839-C	19	7.6 (4.0)	5.3 (0.5)	1.1	0.52 (0.31)	2.4	-0.35
S10-839-LA	8	12.1 (6.0)	5.4 (0.6)	1.2	0.49 (0.24)	2.4	-0.40
S10-839-LC	20	12.5 (3.7)	5.9 (0.6)	1.3	0.61 (0.20)	2.8	-0.42
S12-839-A	20	8.8 (3.5)	5.6 (0.3)	1.1	0.82 (0.27)	4.2	-0.36
S12-839-C	20	8.2 (4.9)	5.9 (0.5)	1.2	0.57 (0.23)	3.4	-0.38
S12-839-LA	20	8.1 (2.8)	5.8 (0.3)	1.1	0.71 (0.31)	3.9	-0.37
S12-839-LC	20	8.5 (2.8)	5.8 (0.4)	1.1	0.75 (0.27)	4.5	-0.37

$N_{\text{refine}}$ , Number of structures produced during sidechain addition;  $R_{\text{sym}}$ , mean self RMSD (Kerr et al., 1994);  $\text{RMSD}_b$ , root mean square deviation of backbone atoms;  $R_{\text{min}}$ , minimum pore radius of ensemble;  $B$ , stereochemical quality of peptide backbone, defined as  $B = a + 2b$ , where  $a$  and  $b$  are the percentage of residues in the "generously allowed" and "disallowed" regions of the Ramachandran plot (Morris et al., 1992);  $M$ , agreement with mutagenesis. Ensembles S10-947-LA and S10-749-A produced no structures in DG/SA and are thus excluded from this table.

contact with/surrounded by the other transmembrane segments of the Kv channel (such as S5 and S6), which would thus shield the short pores of the  $\alpha$ -helix bundle models from the outer lipid environment.

We have employed pore radius profiles to produce estimates of the ionic conductances ( $G_{\text{pred}}$ ) of the H5 region models and present the data in Tables 4 and 5, with distributions of  $G_{\text{pred}}$  for  $\alpha$ -helix bundle and  $\beta$ -barrel configurations presented in Fig. 10.  $G_{\text{pred}}$  values were calculated with a resistivity of 0.775  $\Omega\text{m}$ , which is equivalent to 100 mM KCl solution (Atkins, 1994). The experimental conductance of *Shaker* channels is  $\sim 19$  pS in 100 mM KCl (Heginbotham and MacKinnon, 1993; Tagliatela et al., 1994). Predicted conductances for  $\beta$ -barrel models are rather low

compared to the experimental value, with the majority of ensembles having  $G_{\text{pred}} = \sim 2\text{--}5$  pS, although the S12-947-A ensemble has  $G_{\text{pred}} = 7.8$  pS. In contrast, the  $\alpha$ -helix bundle ensembles have predicted conductances greater than the experimental value, although four ensembles (T2-Val8-C, T2-Val9-A, T4-Val8-C, and T4-Thr10-A) all have  $G_{\text{pred}}$  values of 20–25 pS. Although the pore radius profiles and  $G_{\text{pred}}$  values (Figs. 8 and 10 and Table 4) of  $\beta$ -barrel ensembles are rather low, it should be remembered that these models are produced in vacuo. Molecular dynamics studies of a number of channel models containing explicit water molecules within the pore have demonstrated that the pore radius (and thus  $G_{\text{pred}}$ ) tends to increase upon solvation (Breed et al., 1996; Kerr et al., 1996; Mitton and Sansom,

**TABLE 5** Properties of  $\alpha$ -helix bundle ensembles

Configuration	$B$	$R_{\text{sym}}$ (Å)	$\text{RMSD}_b$ (Å)	$R_{\text{min}}$ (Å)	$G_{\text{pred}}$ (pS)	$M$
T2-Val8-A	2.9 (2.9)	7.1 (1.3)	2.7	2.39 (0.82)	30.4	-0.19
T2-Val8-C	11.3 (3.0)	7.6 (1.7)	2.9	2.05 (1.18)	24.0	-0.25
T2-Val9-A	7.7 (4.1)	8.4 (1.5)	3.1	1.71 (0.85)	21.0	-0.38
T2-Val9-C	6.5 (2.9)	8.6 (1.3)	3.2	2.55 (0.81)	36.0	-0.44
T2-Thr10-A	7.2 (4.2)	8.5 (1.4)	3.2	2.22 (0.95)	28.8	-0.20
T2-Thr10-C	5.8 (2.7)	10.1 (1.4)	3.6	2.92 (0.73)	42.6	-0.26
T2-Met11-A	2.4 (2.6)	9.8 (1.2)	3.6	3.30 (1.00)	53.2	-0.22
T2-Met11-C	14.4 (3.1)	8.8 (1.5)	3.2	3.24 (1.01)	46.6	-0.14
T2-Thr12-A	8.3 (3.3)	9.3 (1.5)	3.3	3.43 (1.02)	53.0	-0.35
T2-Thr12-C	7.3 (2.6)	8.8 (1.3)	3.2	3.26 (1.28)	44.8	-0.42
T3-Val8-A	7.7 (5.5)	8.4 (1.2)	3.1	2.32 (1.03)	29.8	-0.05
T3-Val8-C	13.1 (2.3)	8.4 (1.4)	3.1	2.45 (0.96)	31.8	-0.03
T3-Val9-A	11.0 (3.0)	9.3 (1.4)	3.4	2.09 (0.84)	27.0	-0.05
T3-Val9-C	4.7 (3.2)	8.5 (1.4)	3.1	2.75 (0.90)	40.4	-0.16
T3-Thr10-A	8.2 (3.8)	9.4 (1.6)	3.4	2.53 (0.96)	34.0	-0.20
T3-Thr10-C	6.3 (3.1)	8.4 (1.2)	3.1	2.67 (0.99)	37.2	-0.19
T3-Met11-A	7.5 (3.7)	9.7 (1.5)	3.6	3.17 (0.77)	44.4	-0.21
T3-Met11-C	12.1 (4.9)	9.6 (1.4)	3.5	3.14 (0.79)	40.6	-0.25
T4-Val8-A	6.0 (3.7)	9.2 (1.5)	3.4	2.39 (0.82)	27.2	-0.08
T4-Val8-C	11.4 (3.8)	7.8 (1.2)	3.0	2.05 (1.18)	32.0	+0.01
T4-Val9-A	7.2 (3.6)	8.9 (1.7)	3.4	1.71 (0.85)	32.4	-0.13
T4-Val9-C	9.5 (3.5)	8.6 (1.3)	3.3	2.55 (0.81)	24.0	-0.03
T4-Thr10-A	12.3 (3.9)	9.2 (1.7)	3.4	1.97 (0.85)	23.4	-0.26
T4-Thr10-C	7.8 (3.7)	8.7 (1.3)	3.2	2.33 (0.85)	31.4	-0.26

$R_{\text{sym}}$ ,  $\text{RMSD}_b$ ;  $R_{\text{min}}$ ,  $B$ ,  $M$ , defined as in Table 4. Ensembles contain 24 structures.

1996). Extended MD simulations on Kv channel models with intrapore water molecules, designed to determine whether this may be true for  $\beta$ -barrel models, are under way (Ranatunga, Kerr, and Sansom, unpublished observations). Furthermore, the  $G_{\text{pred}}$  calculations are conducted on models that omit additional elements which may contribute to the pore (e.g., the S5 and S6 segments; Lopez et al., 1994; Shieh and Kirsch, 1994; Tagliatela et al., 1994). However, the value of  $G_{\text{pred}}$  depends to a large extent on the narrowest region of the pore (i.e., that defined by H5), and thus incorporation of S5 and S6 into further molecular models is not expected to significantly effect conductance calculations.

### Overall ranking of models versus experimental mutagenesis data

To rank the 64 ensembles, we must compare their fit to the experimental data. For this comparison we must identify the pore-lining residues of every model in each ensemble. Clearly, a visual inspection of all 1355 models would be somewhat time consuming. Instead, automatic identification of pore-lining residues was achieved by calculating the center of mass of the backbone atoms of each residue, and the center of mass of the side-chain atoms of each residue. For a given residue, if the center of mass of the side chain is closer to the pore axis than the center of mass of the backbone, then this residue is flagged as pore lining. Thus, for each of the 64 ensembles we could identify the percentage of times a residue  $i$  is exposed to the pore, expressed as the Exposure Index,  $e_i$ .

Each ensemble is then scored for the agreement of  $e_i$  with  $P_i$ , the Positional Index for residues within H5 determined from analysis of site-directed and cysteine-mutagenesis data (Table 2). Because  $e_i$  values are on a scale of 0 to 1, and  $P_i$  values range from  $-1$  to  $+2$  (Table 2), the former are normalized to be on the same scale as  $P_i$ . Then, for each residue  $i$  in a given ensemble, the agreement between the normalized exposure index,  $E_i$ , with the positional index,  $P_i$ , is defined as  $M_i$ , where

$$M_i = |E_i - P_i| - 1.5$$

as demonstrated in Table 6. It should be noted that in the following discussion we refer to a "high-scoring bundle" as one with good agreement with the mutagenesis data (i.e., a low value of  $M$ ). The score ( $M$ ) for each ensemble is presented in Tables 4 and 5, with distributions plotted as histograms in Fig. 11. No ensemble shows perfect agreement with the biochemical data. A perfect agreement would yield a score of  $-1.50$ , whereas random agreement would correspond to a score of  $+1.50$ . The data indicate that  $\beta$ -barrel ensembles tend to show slightly better agreement with the data (mean  $M = -0.24 \pm 0.10$ ) than  $\alpha$ -helix bundle configurations (mean  $M = -0.20 \pm 0.12$ ). Interestingly, the agreement over the first half of the H5 region is considerably better for  $\alpha$ -helix bundle configurations than for  $\beta$ -barrels, whereas the converse is true for the C-terminal half of H5. For the two examples shown, the N-terminal and C-terminal scores per residue for S12-839-LA are  $-0.33$  and  $-0.56$ , respectively, and for T2-Val9-A the scores are  $-0.82$  and  $+0.49$ , respectively.

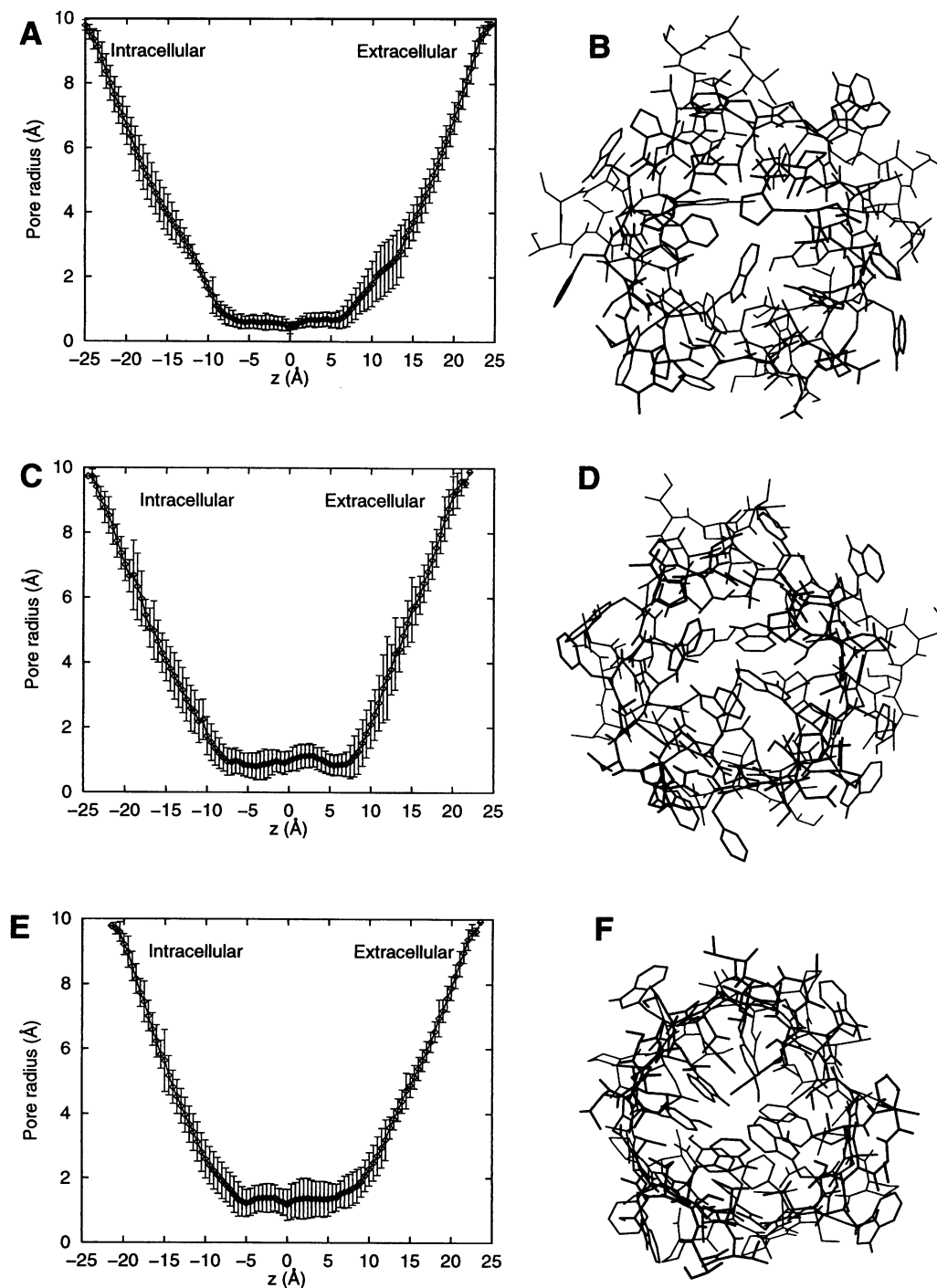


FIGURE 8 Refinement of  $\beta$ -barrel models by simulated annealing and molecular dynamics. (A, B) S12-947-A; (C, D) S10-947-LC; (E, F) S8-839-LC. The pore radius (Smart et al., 1993) is plotted as a function of the distance along the pore axis ( $z$ ) averaged across all 20 members of the ensemble (A, C, E). The corresponding structure diagram is of a representative structure (with a high degree of fourfold symmetry) viewed from the extracellular mouth. The minimum pore radius increases from S8-839-LC ( $R_{\min} = 0.50 \text{ \AA}$ ) to S10-947-LC ( $R_{\min} = 0.80 \text{ \AA}$ ) and S12-947-A ( $R_{\min} = 1.15 \text{ \AA}$ ).

### Analysis of highest-scoring ensembles

Fig. 12 presents a detailed analysis of the pore-lining residues in three selected ensembles. We present the data for structures selected from the highest scoring  $\beta$ -barrel ensemble

(S10-839-LC; Fig. 12 A), from the  $\beta$ -barrel ensemble with the highest  $G_{\text{pred}}$  (S12-947-A; Fig. 12 B), and from the highest scoring  $\alpha$ -helix bundle ensemble (T2-Val9-C; Fig. 12 C). Representative structures are those whose score (or, in the case of S12-947-A, whose  $G_{\text{pred}}$ ) is close to the

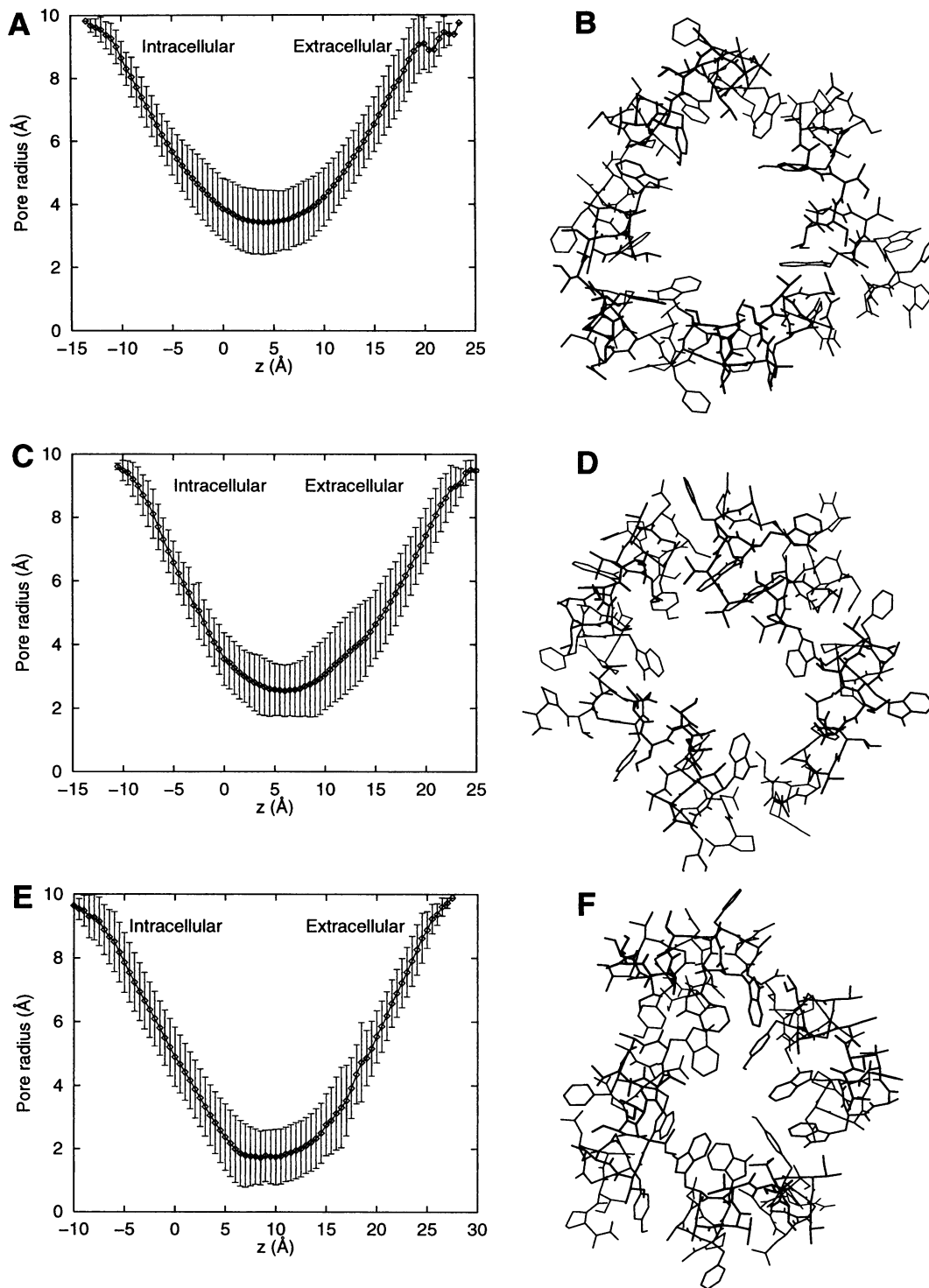


FIGURE 9  $\alpha$ -Helix bundle ensembles. Pore radius profiles are calculated with the program HOLE (Smart et al., 1993) and are displayed as the pore radius calculated along the pore axis ( $z$ ), averaged over the 24 members of each ensemble. A representative structure with a high degree of fourfold symmetry selected from each ensemble is shown from the extracellular side. (A, B) The T2-Thr12-A ensemble has a minimum mean pore radius of 3.4 Å. (C, D) The T2-Val9-C ensemble has a minimum mean pore radius of 2.6 Å. (E, F) The T2-Val9-A ensemble has a minimum mean pore radius of 1.7 Å.

ensemble mean. Residues are colored on the basis of their  $M_i$  values from red (good agreement) to cyan (poor agreement).

The S10-839-LC model selected shows good agreement for pore-lining residues and is lined (and indeed constricted) by the aromatic residues Phe<sup>4</sup>, Trp<sup>6</sup>, and Tyr<sup>16</sup>, of which the

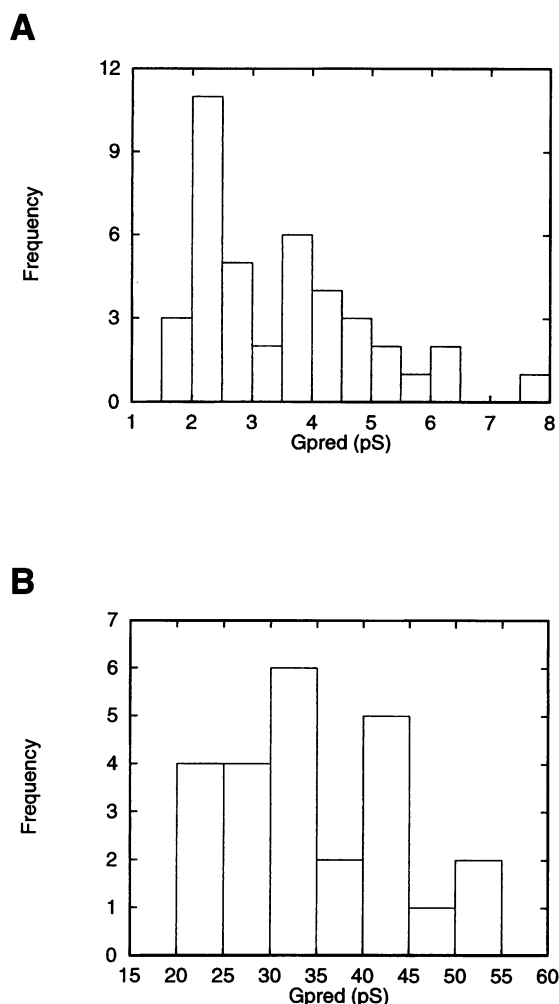


FIGURE 10 Predicted conductance of final ensembles. Conductance was estimated from pore radius profiles as described in the text. Distributions are shown with a 0.5-pS interval for  $\beta$ -barrel configurations (A) and in with a 5-pS interval for  $\alpha$ -helix bundle configurations (B).

tyrosine appears to play a key role in channel selectivity (Heginbotham et al., 1992, 1994). The extracellular mouth of the model is lined by a ring of eight aspartic acid residues that have been demonstrated to be functionally important in CTX and TEA binding (MacKinnon and Miller, 1989; MacKinnon and Yellen, 1990), and the intracellular mouth is lined by threonine residues (Thr<sup>10</sup> and Thr<sup>12</sup>), the latter of which forms part of the internal binding site for TEA (Yellen et al., 1991) and hydroxylamine (Yool and Schwarz, 1995), whereas the former may have a role in the determination of selectivity (Heginbotham et al., 1994). Residues that disagree with mutagenesis data include Trp<sup>5</sup> and Val<sup>8</sup>, the orientations of which (non-pore-lining and pore-lining, respectively) disagree with data obtained by cysteine-scanning mutagenesis (Lü and Miller, 1995), which suggests the opposite orientation for both residues. Val<sup>14</sup>, discussed above, is both exposed to the pore ( $e_i$  value over the ensemble is 0.94) and located  $\sim 75\%$  of the way through the

pore, i.e., close to, but not directly at, the intracellular mouth of the channel.

The considerably wider S12-947-A ensemble (the model in the figure has a pore radius of 1.47 Å) shows poorer agreement with the mutagenesis data. In particular, Phe<sup>4</sup> is now non-pore-lining, which disagrees with data indicating a possible role in ionic selectivity (Yool and Schwarz, 1991), but agrees with Cys-scanning mutagenesis data at the same residue (Kürz et al., 1995; Lü and Miller, 1995). Additionally, Asp<sup>18</sup>, although pore-lining, is deep within the pore, which is in conflict with the accessibility of this residue to external MTS reagents when mutated to Cys (Pascual et al., 1995).

The model selected from the highest scoring helix bundle ensemble (T2-Val9-C) is shown in Fig. 12 C. The lumen of the pore, which has a minimum radius of 1.2 Å, is constricted by Met11 at the intracellular mouth and is lined by the aromatic rings of Phe<sup>16</sup> and Trp<sup>5</sup>. Again, there is a ring of aspartic acid residues at the extracellular mouth contributed by Asp<sup>18</sup>, although this ring is not as exposed as in the S10-938-LC model described above. The other Asp residue (Asp<sup>2</sup>) is not exposed in the T2-Val9-C model ( $e_i$  0.25), which is in conflict with mutagenesis data on this residue, which demonstrate that it is a site of interaction with externally applied TEA and CTX (MacKinnon and Miller, 1989; MacKinnon and Yellen, 1990; Escobar et al., 1993; Gross et al., 1994). The threonine side chains of residue 12 line the intracellular mouth of the channel, in agreement with mutagenesis experiments (Yellen et al., 1991; Yool and Schwarz, 1995). An additional conflict with mutagenesis data is the orientation of Val<sup>14</sup>, which has an  $e_i$  value of 0.5 in this model (and 0.27 across the ensemble), contrary to its identification as a pore-lining residue by both cysteine-scanning (Lü and Miller, 1995) and site-directed mutagenesis (Kirsch et al., 1992; Heginbotham et al., 1994) experiments.

Tables 4 and 5 identify a number of other ensembles that could be candidates for further refinement studies. Of the  $\beta$ -barrel models, it is evident that the ensembles based on an 8-3-9 thread have higher scores than other  $\beta$ -barrel models, and thus selected 8-3-9 models will be the subject of continuing modeling studies. Of the  $\alpha$ -helix bundle models, additional high-scoring ensembles are T2-Val9-A, T2-Thr12-A, and T2-Thr12-C. However, of these, the latter two have very high predicted conductances and pore radii that are difficult to reconcile with high K<sup>+</sup> selectivity, given the crystal radius of a K<sup>+</sup> ion, 1.33 Å (Moore, 1972). Such analyses suggest that further simulation studies may concentrate on  $\beta$ -barrel models rather than on  $\alpha$ -helix bundle models.

## DISCUSSION

### Critique of the methods

There are a number of underlying assumptions in our interpretation of the site-directed mutagenesis and cysteine-scanning

**TABLE 6** Scoring ensembles

S12-839-LA																	
Sequence	D2	A3	F4	W5	W6	A7	V8	T12	T13	V14	G15	Y16	G17	D18	M19	T20	
$P_i$	2	0	0	1	1	-1	-1	1	0	2	0	2	0	2	2	2	
$e_i$	0.91	0.00	0.91	0.00	0.84	0.00	0.89	0.91	0.00	0.91	0.91	0.81	0.91	0.91	0.00	0.91	
$E_i$	1.73	-1.00	1.73	-1.00	1.52	-1.00	1.67	1.73	-1.00	1.73	1.73	1.43	1.73	1.73	-1.00	1.73	
$M_i$	-1.23	-0.50	0.23	0.50	-0.98	-1.50	1.17	-0.77	-0.50	-1.23	0.23	-0.93	0.23	-1.23	1.50	-1.23	
T3-Val9A																	
Sequence	D2	A3	F4	W5	W6	A7	V8	T12	T13	V14	G15	Y16	G17	D18	M19	T20	
$P_i$	2	0	0	1	1	-1	-1	1	0	2	0	2	0	2	2	2	
$e_i$	0.72	0.00	0.03	0.89	0.68	0.01	0.42	0.06	0.81	0.03	1.00	0.68	1.00	0.00	0.06	0.69	
$E_i$	1.16	-1.00	-0.91	1.67	1.04	-0.97	0.26	-0.82	1.43	-0.91	2.00	1.04	2.00	-1.00	-0.82	1.07	
$M_i$	-0.66	-0.50	-0.59	-0.83	-1.46	-1.47	-0.24	0.32	-0.07	1.41	0.50	-0.54	0.50	1.50	1.32	-0.57	

$P_i$ , Positional index for each residue in H5 determined from site-directed and cysteine-scanning mutagenesis data;  $e_i$ , exposure index (see text);  $E_i$ , normalized  $e_i$  values (to be comparable to  $P_i$  values);  $M_i$ , residue score = |normalized  $E_i - P_i$ | - 1.5. The score for the ensemble ( $M$ ) is given by  $\sum M_i/N$ , the number of residues. Note that loop residues and proline residues are not included in the calculation.

ning mutagenesis data that should be discussed. First, we have assumed that all mutagenesis data are the result of a direct effect, i.e., that mutations do not unduly perturb the

structure of the Kv channel. Although it seems unlikely that this is the case for all mutations made in the H5 region, it is an unavoidable assumption to make as we are unable to say unequivocally that a particular mutation must be acting via an indirect structural perturbation. Second, we have interpreted data from many different Kv channels as restraints on models of the *Shaker* Kv channel. This is valid, given that there is a very high degree of conservation in the H5 region between Kv channels from a variety of species (Tempel et al., 1987; Frech et al., 1989; Schachtman et al., 1992; Milkman, 1994), suggesting that the conformation of H5 in different Kv channels is the same. Third, we do not draw any inferences from null mutations (i.e., mutations that result in the failure of a channel to express). This seems a necessary assumption to make, as again we cannot be sure why such a mutant does not express. It may be due to a critical disruption of the channel-lining region, but it may be due to an effect on the overall structure of the channel or resulting from, e.g., a defect in the processing of the newly synthesized protein.

In addition, we have made two assumptions regarding the structure of the H5 region, viz., that H5 adopts a regular, defined secondary structure for its entire length (i.e., either an eight-stranded  $\beta$ -barrel conformation or an eight-staved  $\alpha$ -helix bundle conformation) and that models of H5 generated in the absence of the remainder of the TM region of the protein are valid. The first assumption was made on the grounds that among high-resolution structures for integral membrane proteins, there are no examples of disordered transmembrane structure, with the exception of the L3 loop in porins (Weiss et al., 1991). Although this loop penetrates the porin lumen, it must be remembered that porins are generally nonselective proteins with large, water-filled pores, an environment in which the L3 loop could fold in a nonrepeating conformation. The extremely high selectivity of Kv channels suggests a narrower pore in which less water would be available for the hydration of exposed backbone hydrogen bonding atoms. Thus the adoption of a regular secondary structure in which all backbone hydrogen-bonding groups are satisfied (either by inter-H5-subunit interactions in the case of  $\beta$ -barrels, or by intra-H5-subunit inter-

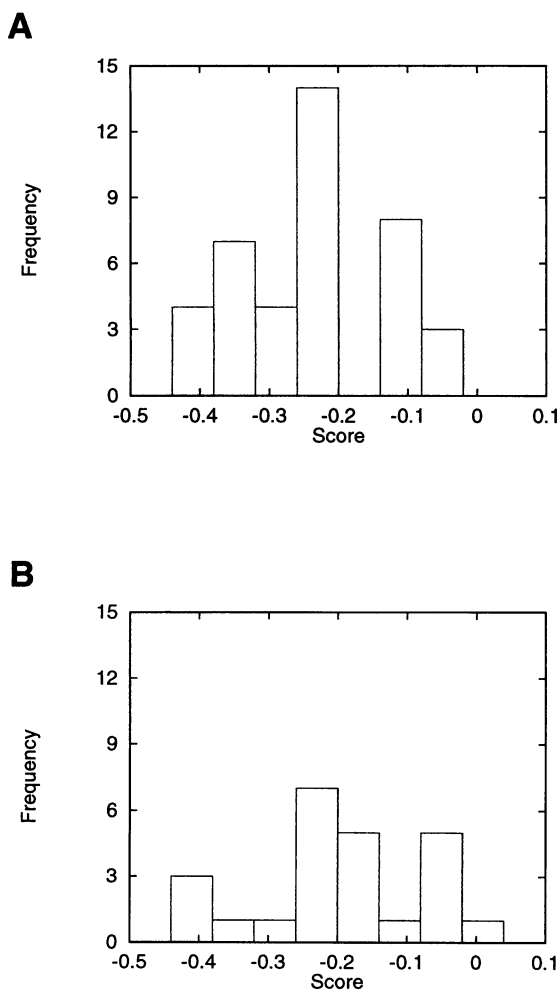


**FIGURE 11** Agreement of ensembles with site-directed mutagenesis data. Ensembles were scored as described in the text. The frequency histogram was calculated with a bin width of 0.05. The distributions are shown in **A** for  $\beta$ -barrel configurations and in **B** for  $\alpha$ -helix bundle configurations.

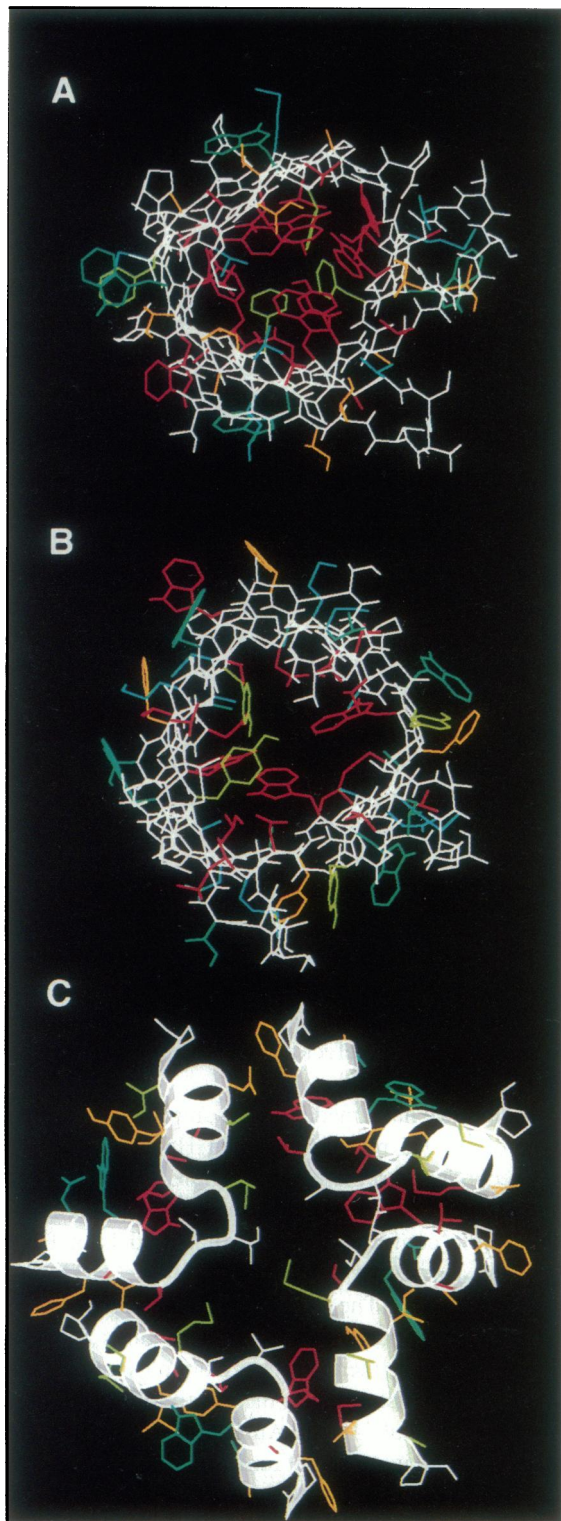


FIGURE 12 Analysis of pore-lining residues of selected ensembles. Representative structures from the highest scoring  $\beta$ -barrel ensemble (S10-839-LC) (A), largest  $G_{\text{pred}}$   $\beta$ -barrel ensemble (S12-947-A) (B), and highest scoring  $\alpha$ -helix bundle ensemble (T2-Val9-C) (C) are displayed as viewed from the intracellular mouth of the channel. Residues are colored for their agreement ( $M_i$ ) with mutagenesis data as follows: red,  $-1.50 < M_i < -0.90$ ; gold,  $-0.90 < M_i < -0.30$ ; lime,  $-0.30 < M_i < +0.30$ ; green,  $+0.30 < M_i < +0.90$ ; cyan,  $+0.90 < M_i < +1.50$ . Residues that are not

actions in the case of  $\alpha$ -helix bundles) would be preferred. However, in the current study, we have not addressed the question of local distortions (e.g.,  $\beta$ -bulges) in otherwise regular secondary structural models that may produce ensembles with lower  $M$  values (Kerr and Sansom, unpublished observations). Our assumption that models of H5 can be generated in the absence of the remainder of the protein is likely to be valid, as we are simply investigating whether there are sufficient site-directed mutagenesis data to determine the conformation of the H5 region. We do not present the H5 models as definitive models of the Kv channel pore and discuss further refinements of the models in a later section.

### Modeling from biochemical data

In this paper we have attempted to produce objective molecular models in the absence of any structural data by employing restraints derived from site-directed mutagenesis data. We have shown that site-directed mutagenesis experiments can be interpreted as topological and orientational restraints and can be combined with secondary structural restraints to produce a small number of candidate models for Kv channel pores. A common question in both globular and membrane protein structure prediction is how accurate modeling can be in the absence of structural information. It has been demonstrated that  $C\alpha$ - $C\alpha$  distance restraints derived from identification of the residues contributing to nonoverlapping, functional epitopes could be employed to screen structural models for human growth hormone (Jin et al., 1994). Such restraints were able to reduce 1388 plausible models to 4, which final models showed an RMSD to the known structure of 4.2 Å. A related study by Lund and colleagues suggested that knowledge of secondary structure, combined with known disulfide arrangements and assignment of surface-exposed residues, could be employed to produce accurate predictions of protein structure only when a single additional distance restraint for each residue in the protein was included in an empirical energy function (Lund et al., 1996).

The application of restraints derived from biochemical and low-resolution structural data to predict membrane protein structure has been demonstrated by a study of bacteriorhodopsin (bR) (Herzyk and Hubbard, 1995). This group interpreted site-directed mutagenesis data, sequence variability data (Donnelly et al., 1993), and interhelix loop lengths as a set of positional and orientational restraints on the seven TM helices of bR. In addition, helix positional and orientational restraints were interpreted from low-resolution electron microscopic data (Henderson and Unwin, 1975). Incorporation of these restraints into a Monte Carlo simu-

scored (i.e., prolines and loop residues) are displayed in white. The backbone is displayed in white for  $\beta$ -barrel models (A, C) and is represented in ribbon form in the  $\alpha$ -helix bundle model (C).

lated annealing protocol, employing a reduced representation of amino acids, produced a model with an RMSD of 1.9 Å to the high-resolution structure of bR (Herzyk and Hubbard, 1995).

The application of restraints derived from electron microscopic data has also been demonstrated for the pore-lining region of the nicotinic acetylcholine receptor. Low-resolution data for the closed (Unwin, 1993) and open (Unwin, 1995) states of the receptor were interpreted in terms of helix axis restraints. By using SA/MD (Kerr et al., 1994), ensembles of models have been produced that are compatible with these restraints and satisfy the results of a large number of biochemical and site-directed mutagenesis experiments (Sansom et al., 1995; Sankararamakrishnan et al., 1996).

We have demonstrated that in the absence of high-resolution structural information, biochemical data can be interpreted in the form of restraints to screen a large number of putative models, thus identifying a set of candidate models for further modeling studies. However, it seems that the Kv channel pore structure is still underdetermined by the available data, and that further distance restraints will be required. Such distance restraints could be derived from a number of sources, including spin-labeling studies (Wu et al., 1996), solid-state NMR spectroscopy (Smith and Peersen, 1992), or disulfide bridge cross-linking (as demonstrated for mapping of helix-helix contacts in rhodopsin; Yu et al., 1995). Alternatively, experiments that estimate the distance between electrostatically interacting residues on CTX and residues in the Kv channel outer vestibule must be used to map the contacts between CTX and the channel (Naranjo and Miller, 1996). The recent determination of the structure of the inactivating "ball" peptide by NMR spectroscopy should form the basis for similar experiments to "map" the binding site of the "ball" peptide at the intracellular mouth of the channel (Antz et al., 1997).

### Comparison with in vitro studies of isolated H5 peptides

A number of studies have concentrated on the structure and function of synthetic peptides corresponding to the H5 region of Kv channels (Peled and Shai, 1993; Haris et al., 1994; Shinozaki et al., 1994). The secondary structure has been quantified by circular dichroism (CD) and Fourier-transform infrared spectroscopy in a variety of aqueous and hydrophobic media, and the potential of H5 to self-associate (Peled and Shai, 1993) and form ion channels in planar lipid bilayers (Haris et al., 1994; Shinozaki et al., 1994) has been documented. The results of such studies have been somewhat ambiguous, as might be anticipated if the secondary structure of the H5 region is determined, in part, by its macromolecular environment. H5 has been reported to contain a high fractional  $\alpha$ -helical content in micelles (Haris et al., 1994) and a high percentage of  $\beta$ -sheet content in aqueous solution and in liposomes (Shinozaki et al., 1994).

A CD study of peptides containing the N- and C-terminal halves of the H5 region, respectively, suggested that in trifluoroethanol/water, the N-terminal segment adopted a predominantly  $\alpha$ -helical structure, whereas the C-terminal region had no defined structure (Peled and Shai, 1993). Furthermore, peptides corresponding to the P-regions from the four repeats of the eel voltage-gated sodium channel have been demonstrated to have an environment-sensitive secondary structure (Cosette et al., 1997).

### Comparison to other models

It is of interest to compare our models with those produced in several previous studies of Kv channels. In principle, our method of restraints interpreted from site-directed mutagenesis data is similar to that employed in a study of  $\beta$ -barrel models of the H5 region performed earlier by Busath and colleagues (Bogusz et al., 1992). This group produced 12 models for the H5 region, all containing an eight-stranded  $\beta$ -barrel. In all cases the shear number ( $S$ ) was 8, and the variables were the position and number of residues in the turn, and the overall orientation of the barrel (i.e., similar to our clockwise and anticlockwise distinction). It is noteworthy that these models, which were generated using restraints derived from only a handful of experimental studies, identified a plausible  $\beta$ -barrel model that would correspond to our S8-839-LA ensemble (Bogusz et al., 1992), a configuration that we have shown still possesses a high degree of agreement with the more extensive mutagenesis data. Additional eight-stranded  $\beta$ -barrels have been constructed by homology modeling to the  $S = 8$   $\beta$ -barrel of superoxide dismutase (Bradley and Richards, 1994). However, from the published data it is not possible to determine precisely the thread of this model, although the pattern of pore-lining residues indicates that it is equivalent to our 9-2-9 or 9-4-7 threads. The  $\beta$ -hairpin model of Jin and Weaver (1993), constructed employing distance restraints to maintain residues 2 and 20 (in our current nomenclature) in a pore-lining orientation, appears to be a thread of 7-4-7 (i.e., similar to our thread 9-4-7), with the N-terminal ends of H5 region unrestrained, to allow residue 2 to be directed toward the lumen. The shear number and orientation of this model are again not deducible from the published data.

Both classes of our models ( $\alpha$ -helix bundle and  $\beta$ -barrel) are somewhat more distinct from the mixed secondary structural models of Kv channel pores that have been presented (Lipkind et al., 1995; Durell and Guy, 1996). In their continuing studies on modeling voltage-gated channels (Guy and Durell, 1995), Guy and colleagues have gradually refined the H5 region of the Kv channel to be consistent with the bulk of the available mutagenesis and pharmacological data (Durell and Guy, 1992, 1996). Their current model bears some similarities to ours in that the H5 region does not fully traverse the lipid bilayer. Rather, the N-terminal half of H5 (residues -1 to 12 in our sequence; see Results) is modeled as an  $\alpha$ -helix, thus satisfying the label-

ing periodicity of the cysteine-scanning mutagenesis experiments (Lü and Miller, 1995), although this helix is not directly lining the pore, whereas the C-terminal half is modeled as random coil for residues 13 to 16, with residues 17 to 19 (Gly-Asp-Met) in a short  $3_{10}$  helix (Durell and Guy, 1996). This model also presents multiple possible potassium ion-binding sites within the pore, in agreement with the multiion nature of potassium channels (Perez-Cornejo and Begenisch, 1994). The other model incorporating mixed secondary structure is that of Fozzard and colleagues (Lipkind et al., 1995). This model incorporates the N-terminal segment of H5 as a  $\beta$ -strand, with the C-terminal half in the conformation  $\beta$ - $\alpha_R$ - $\alpha_L$ - $\alpha_R$ - $\alpha_L$  (where  $\alpha_L$  and  $\alpha_R$  denote the left-handed and right-handed  $\alpha$ -helical region of a Ramachandran plot) for residues Val-Gly-Tyr-Gly-Asp, respectively, thus exposing five consecutive backbone carbonyl oxygens to the pore.

Both of these models incorporate the glycines of the C-terminal half of H5 in nonrepeating secondary structural conformations, reflecting the prevalence of glycine in  $\beta$ -turns and as a traditional secondary structural breaking residue (Richardson and Richardson, 1989). However, the presence of glycine does not preclude regular hydrogen-bonded secondary structures. Indeed, we note that in the *E. coli* outer membrane porin, 11 of 16  $\beta$ -strands contain at least one nonterminal glycine residue, and that the  $\beta$ -hairpin comprising  $\beta$ -strands 9 and 10 of these porins contains six glycine residues in a regular antiparallel hydrogen-bonded conformation (Cowan et al., 1992).

### Extensions to the modeling

We have identified a number of configurations of H5 tetramers (both  $\alpha$ -helix bundle and  $\beta$ -barrel) that have a high degree of agreement with the original mutagenesis data and have a predicted pore conductance comparable to that obtained for *Shaker* Kv channels. These models will be extended in a number of ways. First, the pore properties of the models will be investigated in greater detail by performing molecular dynamics simulations in which the channel lumen is solvated by water molecules. These simulations will thus "refine" the models and allow a detailed analysis of the dynamic and structural features of water molecules within the pore. As we have shown for a number of other systems, MD refinement in the presence of water may result in an increase in pore radius over that of unsolvated models (Breed et al., 1996; Kerr et al., 1996; Mitton and Sansom, 1996). Preliminary simulations indicate that this may also be true for the  $\beta$ -barrel models of Kv channels (Ranatunga, Kerr and Sansom, unpublished observations), with a concomitant increase in  $G_{\text{pred}}$  to values closer to the experimentally determined 19 pS. Simulations can also be performed in the presence of ions to investigate the selectivity of the models (Roux, 1996; Singh et al., 1996). The H5 region models that we have produced require the addition of the remainder of the TM region (i.e., the helices S1–S6). We

have developed a Monte Carlo simulated annealing method to automatically pack TM helices into bundles (Son and Sansom, 1996) and have extended this method to allow the generation of models for S1–S6 with fourfold symmetry and with a hole large enough to accommodate the H5 models described. The results of these simulations will be presented elsewhere (Son, Kerr, and Sansom, manuscript in preparation).

In summary, we have demonstrated how restraints can be derived from site-directed mutagenesis data, and how such restraints can be used to screen a large number of candidate models for the Kv channel pore. Refinement of the models is under way, although more powerful structural restraints may be required to further discriminate between a small number of candidate models.

We thank the Oxford Centre for Molecular Sciences for computational facilities and Dr. Oliver Smart (Birkbeck College) for HOLE.

This work was supported by the Wellcome Trust.

### REFERENCES

- Aiyar, J., A. Nguyen, K. G. Chandy, and S. Grissmer. 1994. The P-region and S6 of Kv3.1 contribute to the formation of the ion conduction pathway. *Biophys. J.* 67:2261–2264.
- Aldrich, R. 1993. Advent of a new family. *Nature*. 362:107.
- Antz, C., M. Geyer, B. Fakler, M. K. Schott, H. R. Guy, R. Frank, J. P. Ruppersberg, and H. R. Kalbitzer. 1997. NMR structure of inactivation gates from mammalian voltage-dependent potassium channels. *Nature*. 385:272–275.
- Atkins, P. W. 1994. *Physical Chemistry*. Oxford University Press, Oxford.
- Baker, E. N., and R. E. Hubbard. 1984. Hydrogen bonding in globular proteins. *Prog. Biophys. Mol. Biol.* 44:97–179.
- Bogusz, S., A. Boxer, and D. D. Busath. 1992. An SS1-SS2  $\beta$ -barrel structure for the voltage-activated potassium channel. *Protein Eng.* 5:285–293.
- Bradley, J. C., and W. G. Richards. 1994. Potassium channels: a computer prediction of structure and selectivity. *Protein Eng.* 7:859–862.
- Breed, J., P. C. Biggin, I. D. Kerr, O. S. Smart, and M. S. P. Sansom. 1997. Alamethicin channels—modelling via restrained molecular dynamics simulations. *Biochim. Biophys. Acta.* 1325:235–249.
- Breed, J., I. D. Kerr, R. Sankaramkrishnan, and M. S. P. Sansom. 1995. Packing interactions in Aib-containing helices: molecular modelling of parallel dimers of simple hydrophobic helices and of alamethicin. *Biopolymers.* 35:639–655.
- Breed, J., R. Sankaramkrishnan, I. D. Kerr, and M. S. P. Sansom. 1996. Molecular dynamics simulations of water within models of ion channels. *Biophys. J.* 70:1643–1661.
- Brooks, B. R., R. E. Bruccoleri, B. D. Olafson, D. J. States, S. Swaminathan, and M. Karplus. 1983. CHARMM: a program for macromolecular energy, minimisation, and dynamics calculations. *J. Comp. Chem.* 4:187–217.
- Brown, A. M. 1993. Functional bases for interpreting amino acid sequences of voltage-dependent K<sup>+</sup> channels. *Annu. Rev. Biophys. Biomol. Struct.* 22:173–198.
- Brünger, A. T. 1992. X-PLOR Version 3.1. A System for X-ray Crystallography and NMR. Yale University Press, New Haven, CT.
- Busch, A. E., R. S. Hurst, R. A. North, J. P. Adelman, and M. P. Kavanaugh. 1991. Current inactivation involves a histidine residue in the pore of the rat lymphocyte potassium channel RgK5. *Biochem. Biophys. Res. Commun.* 179:1384–1390.
- Choi, K. L., C. Mossman, J. Aube, and G. Yellen. 1993. The internal quaternary ammonium receptor site of *Shaker* potassium channels. *Neuron.* 10:533–541.

- Cosette, P., L. Brachais, E. Bernardi, and H. Duclouhier. 1997. Investigating synthetic P-regions from voltage-gated sodium channel at the conformational and functional levels. *Eur. Biophys. J.* 25:275–284.
- Cowan, S. W., T. Schirmer, G. Rummel, M. Steiert, R. Ghosh, R. A. Aputit, J. N. Jansonius, and J. P. Rosenbusch. 1992. Crystal structures explain functional properties of two *E. coli* porins. *Nature.* 358:727–733.
- DeBiasi, M., H. A. Hartmann, J. A. Drewe, M. Tagliatalata, A. M. Brown, and G. E. Kirsch. 1993. Inactivation determined by a single site in K<sup>+</sup> pores. *Pflügers Arch.* 422:354–363.
- Donnelly, D., J. P. Overington, S. V. Ruffle, J. H. A. Nugent, and T. L. Blundell. 1993. Modelling  $\alpha$ -helical transmembrane domains: the calculation and use of substitution tables for lipid-facing residues. *Protein Sci.* 2:55–70.
- Doupnik, C. A., N. Davidson, and H. A. Lester. 1995. The inward rectifier potassium channel family. *Curr. Opin. Neurobiol.* 5:268–277.
- Durell, S. R., and H. R. Guy. 1992. Atomic scale structure and functional models of voltage-gated potassium channels. *Biophys. J.* 62:238–250.
- Durell, S. R., and H. R. Guy. 1996. Structural model of the outer vestibule and selectivity filter of the *Shaker* voltage-gated K<sup>+</sup> channel. *Neuropharmacology.* 35:761–773.
- Escobar, L., M. J. Root, and R. MacKinnon. 1993. Influence of protein surface charge on the bimolecular kinetics of a potassium channel peptide inhibitor. *Biochemistry.* 32:6982–6987.
- Frech, G. C., A. M. J. VanDongen, G. Schuster, and A. M. Brown. 1989. A novel potassium channel with delayed rectifier properties isolated from rat brain by expression cloning. *Nature.* 340:642–645.
- Gross, A., T. Abramson, and R. MacKinnon. 1994. Transfer of the scorpion toxin receptor to an insensitive potassium channel. *Neuron.* 13:961–966.
- Gutman, G. A., and K. G. Chandy. 1993. Nomenclature of mammalian voltage-dependent potassium channel genes. *Sem. Neurosci.* 5:101–106.
- Guy, H. R., and S. R. Durell. 1995. Structural models of Na<sup>+</sup>, Ca<sup>2+</sup>, and K<sup>+</sup> channels. In *Ion Channels and Genetic Diseases*. Rockefeller University Press, New York. 1–16.
- Haris, P. I., B. Ramesh, M. S. P. Sansom, I. D. Kerr, K. S. Srini, and D. Chapman. 1994. Studies of the pore-forming domain of a voltage-gated potassium channel protein. *Protein Eng.* 7:255–262.
- Harris, R. E., and E. Y. Isacoff. 1996. Hydrophobic mutations alter the movement of Mg<sup>2+</sup> in the pore of voltage-gated potassium channels. *Biophys. J.* 71:209–219.
- Hartmann, H. A., G. E. Kirsch, J. A. Drewe, M. Tagliatalata, R. H. Joho, and A. M. Brown. 1991. Exchange of conduction pathways between two related K<sup>+</sup> channels. *Science.* 251:942–945.
- Heginbotham, L., T. Abramson, and R. MacKinnon. 1992. A functional correlation between the pore of distantly related ion channels as revealed by mutant K<sup>+</sup> channels. *Science.* 258:1152–1155.
- Heginbotham, L., Z. Lu, T. Abramson, and R. MacKinnon. 1994. Mutations in the K<sup>+</sup> channel signature sequence. *Biophys. J.* 66:1061–1067.
- Heginbotham, L., and R. MacKinnon. 1992. The aromatic binding site for tetraethylammonium ion on potassium channels. *Neuron.* 8:483–491.
- Heginbotham, L., and R. MacKinnon. 1993. Conduction properties of the cloned *Shaker* K<sup>+</sup> channel. *Biophys. J.* 65:2089–2096.
- Henderson, R., and P. N. T. Unwin. 1975. Three-dimensional model of a purple membrane obtained by electron microscopy. *Nature.* 257:28–32.
- Herzyk, P., and R. E. Hubbard. 1995. Automated method for modeling seven-helix transmembrane receptors from experimental data. *Biophys. J.* 69:2419–2442.
- Hille, B. 1992. *Ionic Channels of Excitable Membranes*, 2nd Ed. Sinauer Associates, Sunderland, MA.
- Ho, K., C. G. Nichols, W. J. Lederer, J. Lytton, P. M. Vassilev, M. V. Kanazirska, and S. C. Hebert. 1993. Cloning and expression of an inwardly rectifying ATP-regulated potassium channel. *Nature.* 362:31–37.
- Hucho, F., V. Tsetlin, and J. Machold. 1996. The emerging three-dimensional structure of a receptor: the nicotinic acetylcholine receptor. *Eur. J. Biochem.* 239:539–557.
- Iwata, S., C. Ostermeier, B. Ludwig, and H. Michel. 1995. Structure at 2.8 Å resolution of cytochrome c oxidase from *Paracoccus denitrificans*. *Nature.* 376:660–667.
- Jin, A. Y., and D. F. Weaver. 1993. A computational model of the HBK2 potassium channel ion pore. *Biochem. Biophys. Res. Commun.* 194:1117–1123.
- Jin, L., F. E. Cohen, and J. A. Wells. 1994. Structure from function: screening structural models with functional data. *Proc. Natl. Acad. Sci. USA.* 91:113–117.
- Kerr, I. D., D. G. Doak, R. Sankaramakrishnan, J. Breed, and M. S. P. Sansom. 1996. Molecular modelling of staphylococcal  $\delta$ -toxin ion channels by restrained molecular dynamics. *Protein Eng.* 9:161–171.
- Kerr, I. D., R. Sankaramakrishnan, O. S. Smart, and M. S. P. Sansom. 1994. Parallel helix bundles and ion channels: molecular modelling via simulated annealing and restrained molecular dynamics. *Biophys. J.* 67:1501–1515.
- Ketchum, K. A., W. J. Joiner, A. J. Sellers, L. K. Kaczmarek, and S. A. N. Goldstein. 1995. A new family of outwardly rectifying potassium channel proteins with two pore domains in tandem. *Nature.* 376:690–695.
- Kirsch, G. E., J. A. Drewe, M. Tagliatalata, R. H. Joho, M. DeBiasi, H. A. Hartmann, and A. M. Brown. 1992. A single nonpolar residue in the deep pore of related K<sup>+</sup> channels acts as a K<sup>+</sup>:Rb<sup>+</sup> conductance switch. *Biophys. J.* 62:136–144.
- Kirsch, G. E., J. M. Pascual, and C.-C. Shieh. 1995. Functional role of a conserved asparagine in the external mouth of voltage-gated potassium channels. *Biophys. J.* 68:1804–1813.
- Kubo, Y., T. J. Baldwin, N. Y. Jan, and L. Y. Jan. 1993. Primary structure and functional expression of a mouse inward rectifier potassium channel. *Nature.* 362:127–133.
- Kuntz, I. D., J. F. Thomason, and C. M. Oshiro. 1989. Distance geometry. *Methods Enzymol.* 177:159–205.
- Kürz, L. L., R. D. Zühlke, H.-J. Zhang, and R. H. Joho. 1995. Side-chain accessibilities in the pore of a K<sup>+</sup> channel probed by sulfhydryl-specific reagents after cysteine-scanning mutagenesis. *Biophys. J.* 68:900–905.
- Lesage, F., E. Guillemare, M. Fink, F. Duprat, M. Lazdunski, G. Romey, and J. Barhanin. 1996. TWIK-1, a ubiquitous human weakly inward rectifying K<sup>+</sup> channel with a novel structure. *EMBO J.* 15:1004–1011.
- Li, M., N. Unwin, K. A. Stauffer, Y. N. Jan, and L. Y. Jan. 1994. Images of purified *Shaker* potassium channels. *Curr. Biol.* 4:110–115.
- Lipkind, G. M., D. A. Hanck, and H. A. Fozzard. 1995. A structural motif for the voltage-gated potassium channel pore. *Proc. Natl. Acad. Sci. USA.* 92:9215–9219.
- Lopez, G. A., Y. H. Jan, and L. Y. Jan. 1994. Evidence that the S6 segment of the *Shaker* voltage gated K<sup>+</sup> channel comprises part of the pore. *Nature.* 367:179–182.
- Lü, Q., and C. Miller. 1995. Silver as a probe of pore-forming residues in a potassium channel. *Science.* 268:304–307.
- Ludewig, U., C. Lorra, O. Pongs, and S. H. Heinemann. 1993. A site accessible to extracellular TEA<sup>+</sup> and K<sup>+</sup> influences intracellular Mg<sup>2+</sup> block of cloned potassium channels. *Eur. Biophys. J.* 22:237–247.
- Lund, O., J. Hansen, S. Brunak, and J. Bohr. 1996. Relationship between protein structure and geometrical constraints. *Protein Sci.* 5:2217–2225.
- MacKinnon, R. 1991. Determination of the subunit stoichiometry of a voltage-activated potassium channel. *Nature.* 350:232–235.
- MacKinnon, R., L. Heginbotham, and T. Abramson. 1990. Mapping the receptor site for charybdotoxin, a pore-blocking potassium channel inhibitor. *Neuron.* 5:767–771.
- MacKinnon, R., and C. Miller. 1989. Mutant potassium channel with altered binding of charybdotoxin, a pore-blocking peptide inhibitor. *Science.* 245:1382–1385.
- MacKinnon, R., and G. Yellen. 1990. Mutations affecting TEA blockade and ion permeation in voltage activated K<sup>+</sup> channels. *Science.* 250:276–279.
- Milkman, R. 1994. An *Escherichia coli* homologue of eukaryotic potassium channel proteins. *Proc. Natl. Acad. Sci. USA.* 91:3510–3514.
- Mitton, P., and M. S. P. Sansom. 1996. Molecular dynamics simulations of ion channels formed by bundles of amphipathic  $\alpha$ -helical peptides. *Eur. Biophys. J.* 25:139–150.
- Moore, W. J. 1972. *Physical Chemistry*, 5th Ed. Longman, London.
- Morris, A. L., M. W. MacArthur, E. G. Hutchinson, and J. M. Thornton. 1992. Stereochemical quality of protein structure coordinates. *Proteins Struct. Funct. Genet.* 12:345–364.

- Murzin, A. G., A. M. Lesk, and C. Chothia. 1994. Principles determining the structure of  $\beta$ -sheet barrels in proteins. I. A theoretical analysis. *J. Mol. Biol.* 236:1369–1381.
- Naranjo, D., and C. Miller. 1996. A strongly interacting pair of residues on the contact surface of charybdotoxin and a *Shaker* K<sup>+</sup> channel. *Neuron*. 16:123–130.
- Nilges, M., and A. T. Brünger. 1991. Automated modelling of coiled coils: application to the GCN4 dimerization region. *Protein Eng.* 4:649–659.
- Pardo, L. A., S. H. Heinemann, H. Terlau, U. Ludewig, C. Lorra, O. Pongs, and W. Stuehmer. 1992. Extracellular K<sup>+</sup> specifically modulates a rat brain K<sup>+</sup> channel. *Proc. Natl. Acad. Sci. USA.* 89:2466–2470.
- Pascual, J. M., C.-C. Shieh, G. E. Kirsch, and A. M. Brown. 1995. Multiple residues specify external tetraethylammonium blockade in voltage-gated potassium channels. *Biophys. J.* 69:428–434.
- Peled, H., and Y. Shai. 1993. Membrane interaction and self assembly within phospholipid membranes of synthetic segments corresponding to the H5 region of the *Shaker* K<sup>+</sup> channel. *Biochemistry.* 32:7879–7885.
- Perez-Cornejo, P., and T. Begenisch. 1994. The multi-ion nature of the pore in *Shaker* K<sup>+</sup> channels. *Biophys. J.* 66:1929–1938.
- Pongs, O. 1992. Molecular biology of voltage-dependent potassium channels. *Physiol. Rev.* 72:S69–S88.
- Richardson, J. S., and D. C. Richardson. 1989. Principles and patterns of protein conformation. In *Prediction of Protein Structure and the Principles of Protein Conformation*. Plenum, New York. 1–98.
- Roux, B. 1996. Valence selectivity of the gramicidin channel: a molecular dynamics free energy perturbation study. *Biophys. J.* 71:3177–3185.
- Sankaramakrishnan, R., C. Adcock, and M. S. P. Sansom. 1996. The pore domain of the nicotinic acetylcholine receptor—molecular modelling, pore dimensions and electrostatics. *Biophys. J.* 71:1659–1671.
- Sansom, M. S. P., and I. D. Kerr. 1995. Transbilayer pores formed by  $\beta$ -barrels: molecular modelling of pore structures and properties. *Biophys. J.* 69:1334–1343.
- Sansom, M. S. P., R. Sankaramakrishnan, and I. D. Kerr. 1995. Modelling membrane proteins using structural restraints. *Nature Struct. Biol.* 2:624–631.
- Schachtman, D. P., J. I. Schroeder, W. J. Lucas, J. A. Anderson, and R. F. Gaber. 1992. Expression of an inward-rectifying potassium channel by the *Arabidopsis KAT1* cDNA. *Science.* 258:1654–1658.
- Shieh, C.-C., and G. E. Kirsch. 1994. Mutational analysis of ion conduction and drug binding sites in the inner mouth of voltage-gated K<sup>+</sup> channels. *Biophys. J.* 67:2316–2325.
- Shinozaki, K., K. Anzai, Y. Kirino, S. Lee, and H. Aoyagi. 1994. Ion channel activity of a synthetic peptide with a primary structure corresponding to the presumed pore forming region of the voltage gated potassium channel. *Biochem. Biophys. Res. Commun.* 198:445–450.
- Sibanda, B. L., T. L. Blundell, and J. M. Thornton. 1989. Conformation of  $\beta$ -hairpins in protein structures: a systematic classification with applications to modelling by homology, electron density fitting and protein engineering. *J. Mol. Biol.* 206:759–777.
- Singh, C., R. Sankaramakrishnan, S. Subramaniam, and E. Jakobsson. 1996. Solvation, water permeation and ionic selectivity of a putative model for the pore region of the voltage-gated sodium channel. *Biophys. J.* 71:2276–2288.
- Smart, O. S., J. Breed, G. R. Smith, and M. S. P. Sansom. 1997. A novel method for structure-based prediction of ion channel conductance properties. *Biophys. J.* 72:1109–1126.
- Smart, O. S., J. M. Goodfellow, and B. A. Wallace. 1993. The pore dimensions of gramicidin A. *Biophys. J.* 65:2455–2460.
- Smith, S. O., and O. B. Peersen. 1992. Solid state NMR approaches to studying membrane protein structure. *Annu. Rev. Biophys. Biomol. Struct.* 21:25–47.
- Son, H. S., and M. S. P. Sansom. 1996. Simulation of the packing of transmembrane  $\alpha$ -helices. *Biochem. Soc. Trans.* 24:S140.
- Tagliatela, M., M. S. Champagne, J. A. Drewe, and A. M. Brown. 1994. Comparison of H<sub>5</sub>, S<sub>6</sub> and H<sub>5</sub>-S<sub>6</sub> exchanges on pore properties of voltage-dependent K<sup>+</sup> channels. *J. Biol. Chem.* 269:13867–13873.
- Tagliatela, M., J. A. Drewe, and A. M. Brown. 1993a. Barium blockade of a clonal potassium channel and its regulation by a critical pore residue. *Mol. Pharmacol.* 44:180–190.
- Tagliatela, M., J. A. Drewe, G. E. Kirsch, M. DeBiasi, H. A. Hartmann, and A. M. Brown. 1993b. Regulation of K<sup>+</sup>/Rb<sup>+</sup> selectivity and internal TEA blockade by mutations at a single site in K<sup>+</sup> pores. *Pflügers Arch.* 423:104–112.
- Tagliatela, M., G. E. Kirsch, A. M. J. VanDongen, J. A. Drewe, H. A. Hartmann, R. H. Joho, E. Stefani, and A. M. Brown. 1992. Gating currents from a delayed rectifier K<sup>+</sup> channels with altered pore structure and function. *Biophys. J.* 62:34–36.
- Tempel, B. L., D. M. Papazian, T. L. Schwarz, Y. N. Jan, and L. Y. Jan. 1987. Sequence of a probable potassium channel component encoded at *Shaker* locus of *Drosophila*. *Science.* 237:770–775.
- Tsukihara, T., H. Aoyama, E. Yamashita, T. Tomizaki, S. Yamaguchi, K. Shinzawa-Itoh, R. Nakashima, R. Yaona, and S. Yoshikawa. 1996. The whole structure of the 13-subunit oxidised cytochrome c oxidase at 2.8 Å. *Science.* 272:1136–1144.
- Unwin, N. 1993. Nicotinic acetylcholine receptor at 9 Å resolution. *J. Mol. Biol.* 229:1101–1124.
- Unwin, N. 1995. Acetylcholine receptor channel imaged in the open state. *Nature.* 373:37–43.
- Weiss, M. S., A. Kreusch, E. Schiltz, U. Nestel, W. Welte, J. Weckesser, and G. E. Schulz. 1991. The structure of porin from *Rhodobacter capsulatus* at 1.8 Å resolution. *FEBS Lett.* 280:379–382.
- Wu, J., and H. R. Kaback. 1996. A general method for determining helix packing in membrane proteins in situ: helices I and II are close to helix VII in the lactose permease of *Escherichia coli*. *Proc. Natl. Acad. Sci. USA.* 93:14498–14502.
- Wu, J., J. Voss, W. L. Hubbell, and H. R. Kaback. 1996. Site-directed spin labeling and chemical crosslinking demonstrate that helix V is close to helices VII and VIII in the lactose permease of *Escherichia coli*. *Proc. Natl. Acad. Sci. USA.* 93:10123–10127.
- Yang, J., Y. N. Jan, and L. Y. Jan. 1995. Determination of the subunit stoichiometry of an inwardly rectifying potassium channel. *Neuron.* 15:1441–1447.
- Yellen, G., M. E. Jurman, T. Abramson, and R. MacKinnon. 1991. Mutations affecting internal TEA blockade identify the probable pore forming region of a K<sup>+</sup> channel. *Science.* 251:939–942.
- Yellen, G., D. Sodickson, T.-Y. Chen, and M. E. Jurman. 1994. An engineered cysteine in the external mouth of a K<sup>+</sup> channel allows inactivation to be modulated by metal binding. *Biophys. J.* 67:1068–1075.
- Yool, A. J., and T. L. Schwarz. 1991. Alteration of ionic selectivity of a K<sup>+</sup> channel by mutation of the H5 region. *Nature.* 349:700–703.
- Yool, A. J., and T. L. Schwarz. 1995. Interactions of the H5 pore region and hydroxylamine with N-type inactivation in the *Shaker* K<sup>+</sup> channel. *Biophys. J.* 68:448–458.
- Yu, H., M. Kono, T. D. McKee, and D. D. Oprea. 1995. A general method for mapping tertiary contacts between amino acid residues in membrane-embedded proteins. *Biochemistry.* 34:14963–14969.